Le informazioni contenute nel presente documento,

titolo: Innovative techniques for conformal doping of semiconductors for applications in micro- and nano-electronics

autore: Sebastiano Caccamo

consegnato mezzo e-mail in data: 15/09/2017

sono strettamente riservate e confidenziali e sono indirizzate esclusivamente al destinatario. In accordo fra il Fornitore (Sebastiano Caccamo) ed il Destinatario (Prof. Neri Fortunato, Dott. Arena Giuseppe e Prof.ssa Maria Grazia Grimaldi) tali informazioni riservate sono divulgate esclusivamente con lo scopo di valutare i requisiti di ammissibilità.

Il Destinatario si impegna a non divulgare a terze parti le Informazioni riservate ricevute dal Fornitore né a utilizzare dette Informazioni per qualsiasi scopo diverso da quello introdotto in questa comunicazione/nota.

Nessun altro diritto, titolo o autorizzazione, esplicita o implicita, d'uso di dette informazioni è concesso al Destinatario.

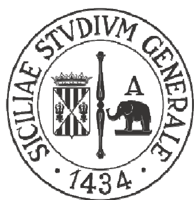

UNIVERSITÀ
degli STUDI
di CATANIA

UNIVERSITÀ DEGLI STUDI DI CATANIA

IN CONVENZIONE CON:

UNIVERSITÀ DEGLI STUDI DI PALERMO

DOTTORATO DI RICERCA IN

Scienza Dei Materiali e Nanotecnologie– XXX CICLO

Sebastiano Caccamo

Innovative techniques for conformal doping of semiconductors for applications in micro- and nano-electronics

---

Tutor: Prof.ssa Maria Grazia Grimaldi
Co-Tutor: Dott.ssa Rosaria Anna Puglisi
Coordinatore: Prof.ssa Maria Grazia Grimaldi

TESI PER IL CONSEGUIMENTO DEL TITOLO DI DOTTORE DI RICERCA

SUMMARY

Preface **... 6**

1 Doping of semiconductors **.. 9**

1.1 Intrinsic Semiconductors and Doping 9

1.2 Existing Doping Techniques 15

1.2.1 Ion implantation (II) and Plasma Immersion Ion implantation (PIII) 15

1.2.2 Diffusion based methods 20

1.2.3 Spin on Dopant (SOD) 21

1.3 Molecular Doping (MD) 22

2 Study of the interface between the molecule and Si in MD 24

2.1 Physical-chemist characterization of the molecules in the standard synthesis conditions 26

2.2 Role of the surface treatments 39

2.3 Role of the dilution of the precursor solution 44

3 Role of the deposition parameters **.................................... 50**

3.1 Role of the coating time and sampling time................ 50

3.2 Role of the solvent and the molecular precursor.......... 56

4 Effects of the post-deposition treatments **.......................... 63**

4.1 Role of the annealing parameters: Temperature and time 64

4.2 Competition between evaporation and diffusion......... 68

4.3 Role of the cap layer 77

5 Example of application to Si nanowires............................. 86

6 Conclusions and future perspectives.................................. 94

Appendix 104

X-Ray Photoelectron Spectroscopy: XPS 104

Spreading Resistance Profiling: SRP 107

Atomic Force Microscopy: AFM 109

Raman Spectroscopy.. 111

References 116

Acknowledgements 125

Publications.. 125

Conferences.. 127

Preface

Silicon is the leading semiconductor material and dominates current micro/nanoelectronics industry.

A fundamental aspect in the development of semiconductor materials and devices is the control of electrically active contaminants (dopants). Over the years the reduction in size and progress in system design of a semiconductor devices required a development of techniques and chemical and physical processes for control of doping on the ever-smaller scale. These have posed constraints for the conventional doping methods (ion implantation and diffusion based method). These methods, indeed, present cost and safety issues, not to count the difficulty to obtain abrupt doping profiles, conformal doping, when the technology requires the dopant atoms to follow 3-D nano-structured surfaces, channelling, charging and crystal damage.

In 2008 a new and low cost technique for controlled and conformal silicon doping for both bulk and nanostructures was reported: Molecular doping (MD)[1,2]. It consists in a monolayer formation during the immersion of the sample in a solution containing dopant precursors and successive annealing to diffuse the dopant.

This Ph.D. thesis is intended to provide a contribution to understanding some aspects of doping by MD through systematic experimental work.

In chapter 1, in order to better understand this work, the main aspects of semiconductor properties, the techniques commonly used for doping these materials and the MD are briefly recalled.

In chapter 2 some aspects of MD are discussed. In particular a physico-chemical characterization of molecular precursors in standard conditions, the role of the surface treatments and the role of the dilution of the precursor solution was examined.

In chapter 3, the results about the role of the deposition parameters in MD are discussed, focusing on the role of coating time and sampling time and on the role of the solvent and the molecular precursor.

Chapter 4 examines the results obtained by studying the effects of the post-deposition treatments. The following aspects are discussed in detail: the role of the annealing parameters: Temperature and time, the competition between evaporation and diffusion and the role of the cap layer.

In chapter 5 an example of application of MD to Si nanowires are investigated.

Finally, the results of this work and the perspectives of this activity are discussed and possible experimental approaches for the study of some unclear aspects in this thesis work are proposed.

These aspects were studied by atomic force microscopy (AFM), X-ray photoelectron spectroscopy (XPS), transmission electronic microscopy (TEM) and Raman Spectroscopy, electrical measurements were performed by spreading resistance profiles (SRP).

1 Doping of semiconductors

In this chapter in order to better understand this thesis, a brief introduction about the semiconductors, the common doping techniques and the MD method will be discussed.

1.1 Intrinsic Semiconductors and Doping

Semiconductors have a monumental impact on our society.

Is possible to find it at the heart of microprocessor chips as well as transistors. Anything that's computerized or uses radio waves depends on semiconductors.

The history of semiconductors is long and complicated and begins in 1782 when Alessandro Volta used the term "semiconductor" for the first time.

The first documented observation of a semiconductor effect is related to Michael Faraday in 1833.

In 1839 Alexander Edmund Becquerel discovered the photovoltaic effect at a junction between a semiconductor and an electrolyte[3]. During the following 100 years many scientists were involved in semiconductor study but it is possible to say that the semiconductors have started to assume an important role in the field of optoelectronics and microelectronics only in 1953, when it was demonstrated that in the p-n junctions if the applied voltage is sufficiently high, there is the multiplication of electrons.

In 1974 the so-called "Law of Moore" was enunciated, in the semiconductor industry, from its creator (at the time head of the Fairchild Semiconductor R&D division and successively founder of Intel) that states that the complexity of micro circuits (which can be measured in the number of chip transistors or unit area) doubled periodically, specifically stated that it did in cycles of about 12 months [4]. The two major factors that made this growth possible were the invention of an integrated circuit that marks the beginning of microelectronics and the benefits that the scaling process can bring to solid state devices. From the '80s to today the technology used mainly to produce microelectronic circuits is provided by the complementary-MOS (CMOS), which is based on devices called the metal-oxide-semiconductor-field-effect transistor (MOSFET). The latter, having a layer of oxide before the gate contact, give at the device the very important feature of isolating the channel from the gate, thus avoiding unwanted current passes. They are produced in planar geometry, meaning that the source, drain and gate contacts are all placed on the same plane and the various areas of different doping are created step by step by a complex process of etching, masking, growth treatments oxides, dopant additions and finally deposition of metals for contacts. Currently, the technology on the market involves choosing a change of geometry from a planar geometry to a three-dimensional type. These new devices have the advantages of scaling, mainly because multi-gate devices allow for greater

channel control. In fact, one of the main problems associated with scaling MOSFET devices is the short channel effect that is caused by the difficulty of controlling the potential, and therefore the current flow in the channel near the gate and the source. [5] However, the production of these devices expects an increase in manufacturing complexity and a greater difficulty in doping. If the planar geometry allowed conventional doping methods in the case of three-dimensional geometries this is no longer possible.

The evolution of semiconductor technologies was determined both by the chemical properties of available materials and by the electrical properties. In the field of solid state physics, semiconductors are defined as solids in which 0 K (and no external excitation) valence band is completely full. It is well known that electrical conduction in solids occurs only when there is a non-fully-fledged electronic state band, so conduction in pure semiconductors occurs only when the electrons have been excited (thermally, optically, etc.) and brought to the bands at Higher energy.

At room temperature, a portion of electrons (generally very small but not negligible) in a semiconductor are thermally excited and carried by the "bandwidth" to the "conduction band". The ease with which electrons can be carried from the band to the conduction band depend on the energy gap between the bands, and is the magnitude of this energy gap serving as a parameter to

divide the semiconductors from the insulators. The energy to break a bond and release an electron is 0.75 eV in the germanium, 1.12 eV in the silicon, while, by comparison, for the electrons of an insulator we will need about 10 eV to free one. In this regard, the temperature plays a very important role since increasing of the thermal agitation of the atoms and therefore of valence electrons, which are therefore able to better cross the threshold of the energy gap.

When electrons are carried by the valence band to the conduction band in a semiconductor, both bands contribute to conduction, because conduction can occur in every non-full energy band. Electrons in the conduction band are called "free electrons", although they are often simply called "electrons" if the context allows them to be clear. Free energy states in the valence band are called "holes".

Solid energy bands are a set of energy levels accessible or not by the electrons within the lattice, and mainly result in two: the valence band and the conduction band. In **Errore. L'origine riferimento non è stata trovata.** we can see the possible situations of the bands in the insulators (a), in the Semiconductors (b) and conductors (c, d).

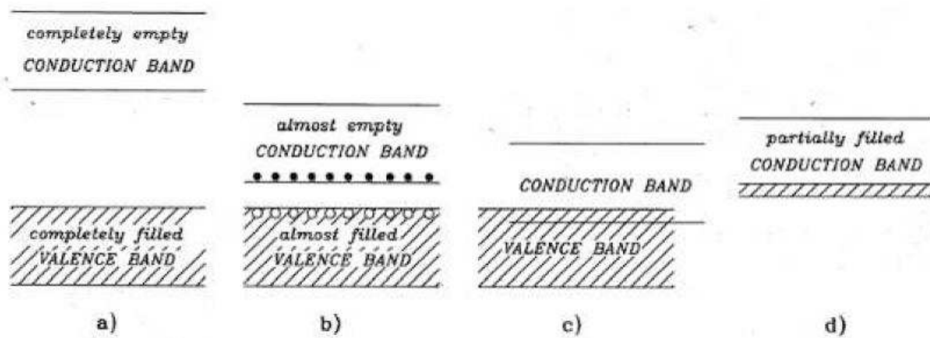

Figure 1-1 Model bands in solid state

One of the main reasons why semiconductors are used in electronics is due to the ability to modify their electronic properties in a highly controlled manner by adding small amounts of impurities called dopant, which can be classified into two types: those that provide an excess of electrons to the conduction band, and those that provide an excess of holes to the valence band. A semiconductor with excess electrons is called semiconductor n-type, while a semiconductor with an excess of gaps is called semiconductor p-type. The band structure is therefore modified and energy levels are introduced in the gap. Silicon and germanium are both tetravalent semiconductors and share their four valence electrons with the first four neighbors (**Errore. L'origine riferimento non è stata trovata.Errore. L'origine riferimento non è stata trovata.**(a)). The purpose of n-type doping is to produce excess electrons in the material. To understand how to do n-type doping, consider the case of silicon

(Si). The atoms of Si have four valence electrons, each of which is covalently linked to one of the four adjacent Si's atoms. If an atom with five valence electrons, as one of the group VA of the periodic table (i.e. phosphorus (P), Arsenic (As), or antimony (Sb)) is incorporated into the crystalline lattice instead of a Si atom, then that atom will have four covalent bonds and a non-covalently bonded electron. (**Errore. L'origine riferimento non è stata trovata.**(b)). This extra electron is only weakly bound to the atom and can easily be brought into the conduction band. Already at normal temperatures practically these electrons in the conduction band. Since the excitation of these electrons does not create holes in the valence band, the number of electrons in these materials is higher than that of the holes. In this case, electrons are the major charge carriers and gaps the minority carriers. Because the atoms to five outer electrons have an electron from "donate", these atoms are indicated with the name of atoms "donor". The purpose of p-type doping is to produce an excess of holes in the material. In the case of silicon, a trivalent atom, such as boron, replaces an atom of Si in the crystalline lattice. The result is that an electron of silicon is missing from one of the possible four covalent bonds. In this way, the atom dopant (boron) can accept an electron from the valence band to complete the fourth bond: this generates the formation of a gap. These dopants are called "acceptors". When a sufficiently large number of acceptor is added, the gaps become more numerous free electrons. Thus, the

gaps are the majority charge carriers, while electrons are the minority charge carriers in p-type materials. (**Errore. L'origine riferimento non è stata trovata.** (c)).

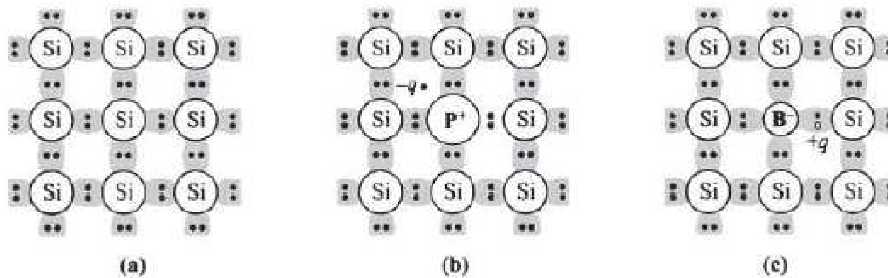

Figure 1-2 Three types of silicon: (a) intrinsic without impurities, (b) n-type silicon doped with phosphorus, (c) p-type silicon doped with boron

1.2 Existing Doping Techniques

In this subsection, the common doping techniques, Ion Implantation (I.I) and plasma immersion ion implantation, diffusion based method, and Spin on Dopant (SOD), with the relative advantages and defects are described.

1.2.1 Ion implantation (II) and Plasma Immersion Ion implantation (PIII)

Ion implantation is the main semiconductor doping method since the 1970s[6–8]. Is a low-temperature process for injecting ions of any element into any solid material, resulting in desirable modification in its chemical, electrical, optical and mechanical

properties. For semiconductor applications, it is extensively used for selectively doping silicon wafers in precise control and for depth profiles of specific impurities. Operating at low temperature the lateral diffusion is negligible and is compatible with conventional lithographic processes, so small regions can be doped. Figure 1-3 Ion implantation systemshowed an Ion implantation system. In this system the precursor of the dopant wanted is introduced into the ionization chamber in which the free electrons, which are generated by thermionic effect, are accelerated under the influence of an electric field, by bombarding the molecules of the gas that is ionized by generating the desired ions.

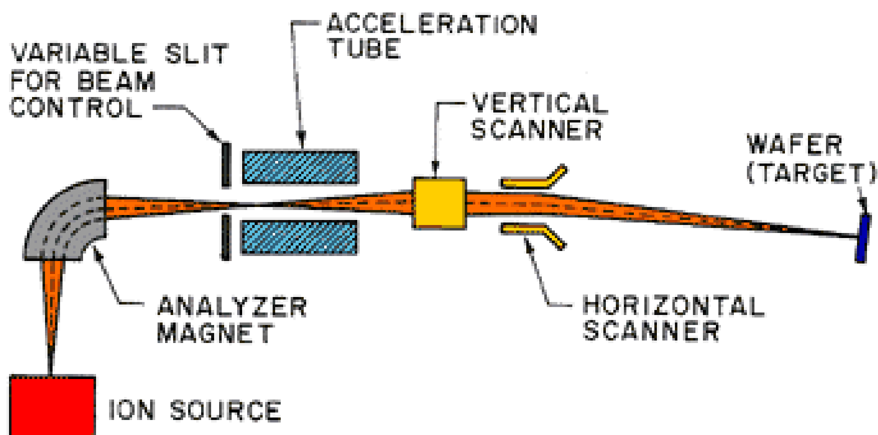

Figure 1-3 Ion implantation system

The dopant ions irradiating the sample are accelerated with high energies ranging from a few tens of eV to the MeV. Using this type of doping, the maximum dopant concentration is found

within the semiconductor and the profile of the dopant distribution is mainly determined by the mass and energy of the implanted ions, the plant angle, the rigidity and the atomic density of the matrix undergoing the implant. In ion implantation, since the wafer surface is impacted by high energy ions, it can cause damage by knocking Si atoms from their position, causing local structural damage. This needs a post thermal annealing treatment to repair the damage.

There are two ways of doing this:

1. Tube furnace - low temperature annealing (600-1000 ◦C). To minimize lateral diffusion.

2. Rapid thermal annealing - higher temperatures are possible but for shorter times.

This technique shows a several issues:

Crystallographic damage: Each individual ion produces many point defects in the target crystal on the impact such as vacancies and interstitials.

Amorphization: The amount of crystallographic damage can be enough to completely amorphize the surface of the target.

Sputtering: Some of the collision events result in atoms being ejected (sputtered) from the surface, and thus ion implantation will slowly etch away a surface. The effect is only appreciable for very large doses.

Ion channeling: Crystallographic directions offer much lower stopping than other directions. The result is that the range of an ion can be much longer if the ion travels exactly along a particular direction. For this reason, most implantation is carried out a few degrees off-axis, where tiny alignment errors will have more predictable effects.

Plasma immersion ion implantation (PIII) [9–11]is an upgrade of ion implantation technique in which the ions were extracted and accelerated from the plasma by applying a high voltage pulsed or pure DC power supply and targeting them into a suitable substrate or electrode with a semiconductor wafer placed over it, so as to implant it with suitable dopants. The electrode is a cathode for an electropositive plasma, while it is an anode for an electronegative plasma. Plasma can be generated in a suitably designed vacuum chamber with the help of various plasma sources. Figure 1-4 shows a PIII system. During the PIII process a component is immersed in a processing plasma discharge containing the desired species, and negative high-voltage pulses are applied directly to the component. Ions are extracted from the plasma and are implanted into the material's surface.

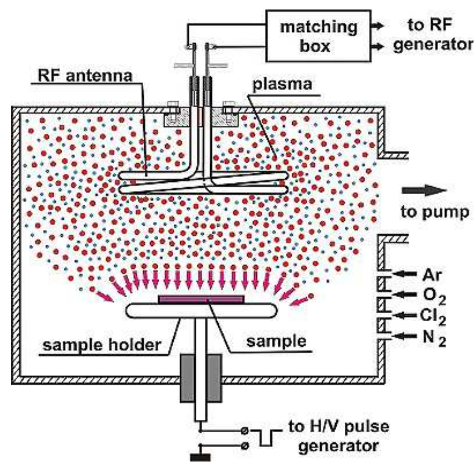

Figure 1-4 Plasma immersion ion implantation system

The ion beam current density depends both on the plasma parameters and the bias voltage and is of the order of 1 – 10 mA/cm^2. A pulsed high voltage is used to reduce substrate heating as well as to control charging. Typical pulse lengths are in the range of 2 to 100 µs at frequencies of a few 100 Hz up to 3 kHz. The substrate temperature can be controlled by varying the implant parameters, and may range from room temperature to 600°C without additional heating. Self-regulating charge control achieved by the alternating attraction of ions and electrons enables one to process not only conductive, but also insulating surfaces. PIII technique has been developed in an effort to obtain increased ion current densities and to reduce both the implant time and the line-of-sight inherent to the conventional beam line ion implantation process. PIII efficiency is superior compared to the standard implantation process, particularly for Low-temperature

process, low energy, Less Hazardous System and high dose implants. Despite these advantages, this technique shows the following drawbacks:

- Possible unwanted impurities present in the plasma into the target can be implanted in addition to the desired dopants.

- Secondary electrons limit the efficiency and generate x-rays.

- Limitation to check dose in situ

- Implant energy distribution is inhomogeneous.

1.2.2 Diffusion based methods

In the diffusion process semiconductor wafers are kept in a high temperature quartz tube furnace, and an appropriate gas mixture is passed.

Thermal diffusion is a two-step process:

1. Deposition - dopant atoms are introduced at the wafer surface.

2. Drive-in - the dopant atoms then diffuse into the wafer to create the required concentration gradient.

Boron is the most common p-type impurity in silicon, whereas arsenic and phosphorus are used extensively as n-type dopant. These three elements are highly soluble in silicon with solubility exceeding 5×10^{20} atoms / cm^3 in the diffusion temperature range (between 800° C and 1200° C). These dopants can be introduced via several means, including solid sources (BN for B, As_2O_3 for

As, and P_2O_5 for P), liquid sources (BBr_3, $AsCl_3$, and $POCl_3$), and gaseous sources (B_2H_6, AsH_3, and PH_3). For liquid and gaseous sources, a concentration of the dopant vapor should be established at the surface. In a liquid source case, a carrier gas is usually used to transport the vapors to the diffusion furnace (e.g. N_2) and is then reduced at the surface. In solid sources case, wafer sized "slugs" are packed into the furnace along with the product wafers (e.g. for boron, boron nitride slugs can be used as solid sources), this is called a solid neighbor source. The number of dopant atoms diffusing in the wafer are proportional to the partial pressure of dopant impurity in the gas mixture. The doping concentration decreases monotonically from the surface, and the in-depth distribution of the dopant is determined mainly by the temperature and diffusion time[12,13]. The pros of this technique are: the lack of damage in the crystal lattice and can be used to batch fabrication. The cons related at this techniques are: Diffusion is bonded to solid solubility, the process needed high temperature, s difficult to create shallow junctions.

1.2.3 Spin on Dopant (SOD)

Spin-on dopants (SOD) provide an impurity source for semiconductor junction fabrication. This method permits a precise control of dopant entering the silicon through application of a homogeneous solution to the substrate using a spin coating method. In this process, no storage of source wafers or use of

costly ion implant equipment is used. After the film deposition over the substrate a diffusion step is performed at high temperature to yield desired sheet resistance and junction depth[14–16]. The cons of this technique are: diffusion of unwanted materials together the desired dopants, difficult to cover not-linear surface and like in the diffusion technique also this case suffer of the limitation to solid solubility and needed high temperature.

1.3 Molecular Doping (MD)

Recently an alternative, easy and low cost strategy to out match the standard doping methods has been proposed: the Molecular Doping (MD) [1]. It is based on the interaction between a molecular precursor containing the dopant atom and the Si surface. The substrate is immersed in a solution containing the molecular precursor. After the deposition time, typically 2.5 hours, on the substrate surface a layer of molecules was formed, with a final surface density strictly correlated to the molecular footprint, i.e. through a self-limiting process [1]. After this step the sample is covered by silicon oxide for protection and annealed in order to decompose the molecule and diffuse the dopant atoms inside Si, with kinetics driven by the diffusion phenomena. The MD is based on a process that involves the use of liquid precursors, this is an advantage which can be exploited for example in the doping of the nanostructures. MD can provide n- and p-type doping and a range of dopant doses, diffusion depths and resistivity controlled

by the molecular structure and design, the deposition conditions and the thermal budget [1,2,17–21]. Metallurgical junctions as small as 5 nm and 10 nm have been demonstrated respectively for n^+ and p^+ doping, and electrical resistivity maps have shown that the wafer-scale uniformity bottle-neck is represented by the annealing process homogeneity[22,23]. The molecular precursor has been applied on planar, micro- and nano-structured surfaces and subjected to the diffusion thermal treatment [21,24–26] demonstrating the absence of crystal damage. The MD layer can also performed using a sacrificial target which is then put in contact with the substrate to be doped, in the so called contact doping method, where the molecules volatize upon annealing and then interact with Si in a fashion similar to the classic gas source methods [27,28].

2 Study of the interface between the molecule and Si in MD

Silicon has undoubtedly been for decades the leading actor among the other semiconductor materials thanks to its abundance, stability and non-toxicity, and the projections confirm this supremacy also for the next years. In addition, the semiconductor roadmap miniaturization objectives are low cost and sustainable production. These have posed constraints for the doping process, i.e. the introduction of the dopant impurities into the intrinsic semiconductor with the function to modulate its electrical properties. Conventional doping methods (ion implantation or diffusion based method) present cost and safety issues, not to count the difficulty to obtain abrupt doping profiles, conformal doping, when the technology requires the dopant atoms to follow 3-D nano-structured surfaces, channelling, charging and crystal damage. MD was showed for the first time in 2008 as an alternative and low cost method in a work of professor Javey and his group[1]. Is based on the interaction between a molecular precursor containing the dopant atom and the Si surface. The substrate is immersed in a solution containing the molecular precursor for a typically deposition time of 2.5 hours and on the substrate surface a layer of molecules was formed. After this step, the sample is covered by silicon oxide for protection and annealed in order to decompose the molecule and diffuse the dopant atoms

inside Si, with kinetics driven by the diffusion phenomena. The MD is based on a process that involves the use of liquid precursors, this is an advantage which can be exploited for example in the doping of the nanostructures. MD can provide n- and p-type doping and a range of dopant doses, diffusion depths and resistivity controlled by the molecular structure and design, the deposition conditions and the thermal budget [1,2,17–21]. MD has been applied on planar, micro- and nano-structured surfaces demonstrating the absence of crystal damage. The MD process can also performed using a sacrificial target which is then put in contact with the substrate to be doped, in the so called contact doping method. The interaction between the molecule and Si in the solution-based MD approach is the crucial point to be studied to deeply understand the mechanisms associated with the MD process.

In particular in this chapter, the following points are discussed in detail:

- study of the physics-chemical characteristics of the molecules in the standard synthesis conditions
- study of the bond after different surface treatments
- study about the dependence of MD on the concentration of the molecular precursor in the solution.

2.1 Physical-chemist characterization of the molecules in the standard synthesis conditions

Semiconductor doping through solution-based self-assembling provides a simple, scalable, and cost-effective alternative to standard methods and additionally allows conformality on structured surfaces. Among the several solution-based deposition techniques, dip coating is the most promising. It consists in immersing the target to be doped inside a solution containing the dopant precursor. During this process, the molecule bonds to the target surface with a self-limiting process ruled by its steric properties. Successive annealing leads to layer decomposition and diffusion of dopant atoms inside the substrate. Most of the work on molecular doping lacks information on the molecule/Si interface chemical properties, on the mechanisms of the molecule evolution during the coating, and of its decomposition after the diffusion step. Moreover, it has so far been devoted to the molecules design to tune the final dopant dose and distribution. In this paragraph, new findings on the interface characteristics in terms of mono and multilayers formation are presented. A systematic study by varying the coating conditions was carried out, demonstrating that the main parameters such as carrier dose, junction depth and sheet resistance can be controlled precisely and that uniformity can be achieved at the nanometer level. [29,30]. The substrate mostly used in this kind of process is Si [25,31–33] but

in literature are present work that involved the use of several substrates such as InAs, InGaAs oxidized silicon, alumina, and mica to study the molecule anchoring mechanisms [29,30,34,35]. The dopant atoms typically injected in the MD are phosphorus, boron, sulfur and in recent work nitrogen arsenic or antimony was used too. The precursor source molecules are several. Octadecylphosphonic acid (OPA) molecules were deposited by dip coating [36–38] or drop casting [39] on a Si surface. In these work, the drop lateral diffusion over the surface during the days after the drop casting was studied by changing the substrate temperature. The result showed a surface redistribution of the molecules and it has been attributed to their amphiphilic nature [40]. The authors found that the molecules were organized in bi- or multiple layers containing always an odd number of it (3,5,7. . .). This behavior is due to the polar nature of the molecules, bonded to the substrate thanks to the polar head, and with the nonpolar tails attached to the successive molecule. Another study on OPA molecules showed the important role of the solvent in the formation of self-assembled monolayers of OPA on oxide surfaces [40]. Changing the solvent polarity, it is possible to determine a total coverage of OPA on substrate surface (using non-polar solvent) or not at all (using a polar solvent). Self-assembled monolayers OPA have also been obtained by T-BAG method on oxide-covered silicon samples [41,42]. The characterization of this T-BAG process was performed by X-ray photoelectron spectroscopy (XPS) [41]. A bulk

film of OPA is deposited after the T-BAG process, performed at room temperature and after baking at 140°C, the layer is converted to a multilayer, with a first one chemically bonded to the substrate and the rest only weakly bonded. The not chemically bonded multi layers are removed after rinsing and a total coverage of single monolayer is obtained after three cycles of deposition, baking, and rinsing. The identification of a tridentate bond between the P atom and three oxygen atoms is deduced from the single component of the P signal. All of these studies evidence the possibility of the formation of mono- or multilayers of molecules through MD, and this controls the amount of initial dose of dopant and of the final incorporated dopant in the substrate, and the importance of the synthesis conditions. In this part of my work, an experimental investigation of MD by focusing on the chemical surface properties and on the coating process conditions will be presented. The morphological and chemical characteristics of the as-deposited molecule and its interactions with the substrate are obtained by performing atomic force microscopy (AFM) and XPS with the goal to demonstrate the presence of the self-assembled monolayers and the molecule modification after the dip coating deposition and after the activation annealing.

The MD procedures found in literature usually start with the dipping of the samples in a 16% HF solution for 60 second to remove the native silicon oxide followed by immersion in 20%

v/v solution of diethyl 1-propylphosphonate and mesitylene at the solution boiling temperature, about 160 °C, for 2.5 h [1,2,25,34]. This step creates layers of phosphorus-containing molecules all over the sample surface (Figure 2-1a). In case of p-type doping, a boron precursor, such as the allylboronic acid pinacol ester (ABAPE), mixed in mesitylene is used at its boiling temperature of about 120 °C [24].

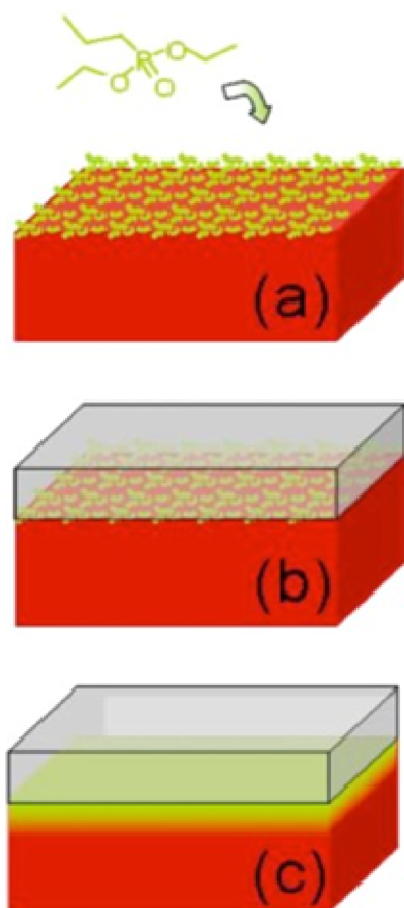

Figure 2-1 Schematic model representing the steps for the molecular doping based on the self-assembling coating process

The samples, after the reaction, are immediately capped with a SiO2 layer deposited by spin on glass (SOG) procedure [2,24,25] (Figure 2-1b). In particular the samples after the molecular deposition have been baked at 80 °C for 60 s on a hot plate, and then covered by SOG oxide deposited by spin coating at 3000 rpm for 20 s. A subsequent baking step at 250 °C for 60 s in air and a last annealing step in the furnace to compact the SOG layer at 425 °C for 1h under 2l/min flow of N_2 were then performed. This process is indicated in the literature as a protection of the dopant molecules and the sample surface from air exposure and from the "escape" of the dopant during the subsequent activation annealing step. A furnace or RTA annealing at temperatures ranging between 900 and 1100 °C for times between 5 and 500 s is then performed to diffuse and activate the dopant (Figure 2-1c). The aspect related to the surface morphology after the deposition of the precursor molecules, especially in terms of formation of mono- or multilayers, has been investigated and debated in the literature. The results present so far, as discussed in the introduction, essentially show that the surface morphology strongly depends on the deposition methodology used. The morphology of the Si substrate after the molecules deposition has been tested also for the dip coating technique.

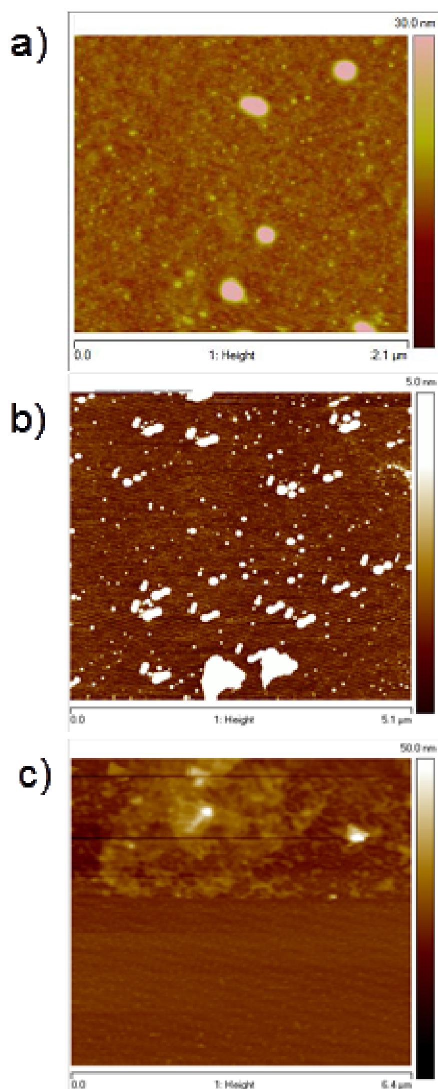

Figure 2-2 AFM micrographs of Si substrates after dip coating in the solution composed of the molecule and mesitylene (a) and only the mesitylene (b). Map of the deposited layer in the region subjected to scratch test by AFM tip (c).

AFM maps have been acquired, by using a DI3100 atomic force microscope, on a sample “as-deposited” (Figure 2-2 a), i.e., after the coating process and without any further treatment such as deposition of the cap layer or annealing process. The topographical map shows that, besides a small roughness that can be correlated to the deposited molecules circular agglomerates with variable size are present. To attribute the presence of the agglomerates to the molecules or to possible other contaminants, such as solvent residuals or decomposition products, AFM measurements were performed on samples immersed in a solution containing only the solvent and by using the same coating conditions. The data are shown in Figure 2-2 b and as can be seen also, in this case, the agglomerates are present while the roughness has disappeared. So, it is possible to attribute their presence to some solvent residuals. This can be expected since the solvent used presents a degree of purity of 98 %. Electronic grade chemicals should be used to overcome this issue. To investigate the thickness of the deposited layer, a scratch with the AFM tip was performed by impressing a force onto the surface by the movement of the AFM tip in contact mode on a restricted area of the sample (Figure 2-2 c). The height of the step formed, corresponding to the thickness of the deposited layer, was measured and resulted in being less than 2 nm, which coincides with the value of the expected thickness of a monolayer of diethyl-1-propylphosphonate [43]. To further investigate the

formation of the self-assembled monolayer and its chemical bonding with the substrate, XPS measurements on the as-deposited samples with a base pressure of 2×10^{-10} torr were performed. A monochromatic Al Ka radiation was employed as the excitation source. XPS spectra at 108 photoelectron angles (relative to the sample surface) were collected, to increase the surface sensitivity of the analysis. In Figure 2-3, the spectra of the C1s (a) and P2p (b) are displayed. The C1s spectra can be deconvoluted in 4 components: the main peak is centered at about 285.4 eV and is attributed to the presence of monolayers chemically bonded to the Si surface [41], a second component at higher binding energy, 286.5 eV, indicate the presence of some residual non-chemically bonded multilayers, while the peaks at 287.5 and 289 eV are attributed to oxidation species such as C–O and C=O, respectively. Figure 2-3 b shows that the P2p signal is constituted by a single component centered at 135 eV. The literature data reports the signal for not oxidized P species at 130 eV [44,45], while our experimental peak position indicates that the P is bonded to an electronegative atom in this case oxygen. It is possible to propose a hypothesis for the anchoring of the molecule. In fact, observing the P2p peak, it is symmetrical. The fact that the peak is symmetric indicates that it consists of a single contribution and suggests that there is only one type of bond between O and P, presumably due to the breakup of the double bond P = O and the simultaneous breaking of the C-O-P bonds. In

the literature, a tridentate model for similar molecules is proposed [41]. If so, the aliphatic portion of the molecule detaches during the coating process, forming some compounds, and the remainder of the phosphorus molecule is bound via oxygen to the substrate.

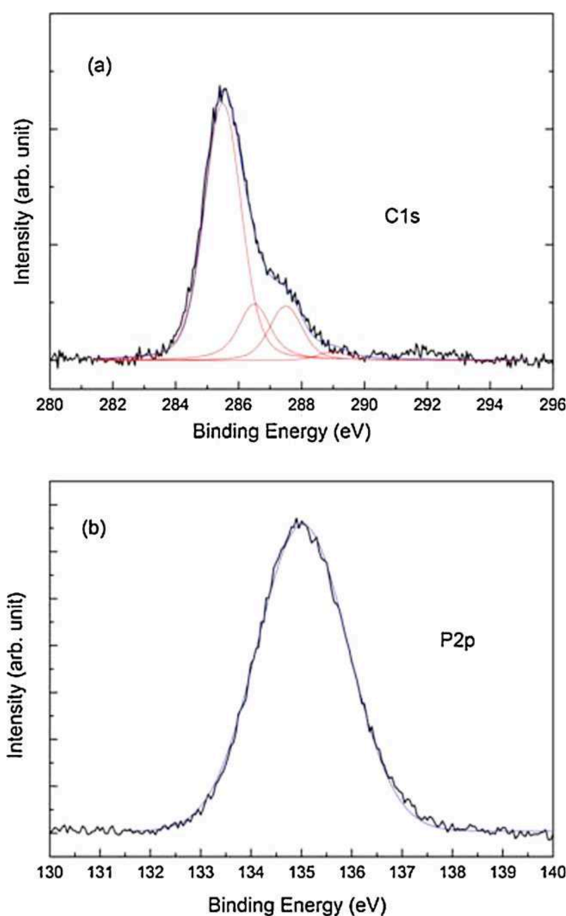

Figure 2-3 XPS spectra relative to the C1s (a) and to the P2p (b) signals acquired on the as-deposited sample.

To investigate the decomposition of the molecule, Raman analysis in the as-deposited samples and after the activation step has been

performed. The relative spectra are shown in Fig. 4. The results display vibrational features in two well different regions: the first one, between 1000 and 1500 cm^{-1}, associated to the deformations of methylene (CH_2) chain and to terminal methyl (CH_3), and the second one in the wavelength region of 2800–3000 cm^{-1} where symmetric and asymmetric stretching modes of the CH_2 and CH_3 units are visible. Note that unfortunately deformations, twisting and rocking modes of alkyl groups overlap the P=O and P–O–C_2H_5 vibrational bands which fall between 1000 and 1300 cm^{-1}. Therefore, it was not possible to evidence the molecule structural changes after anchoring to the Si substrate by exploiting vibrational features of phosphorus containing groups. Moreover, at higher frequencies four prominent bands can be assigned to the C–H stretching modes of the CH_2 and CH_3 groups. In the as-deposited sample (red curve), the symmetric and asymmetric stretching modes of the methylene groups are positioned, respectively, at 2846 and 2912 cm^{-1}, while the symmetric and anti-symmetric stretching modes of the methyl groups were observed at 2879 and 2958 cm^{-1}, respectively. After the high-temperature thermal treatment, i.e., the activation step (black curve), CH_2 stretching mode shifts in the positions toward higher frequency while CH_3 remains almost invariant. Moreover, a change of overall relative intensities was also observed. The CH_2 stretching modes in the alkyl chains are conformational order dependent shifting to higher frequencies at higher conformational

disorder [38–40]. In addition, a mode at 1735 cm^{-1} was observed in both samples. This frequency is correlated to the stretching vibration of C=O of alkyl propionates species, so we can hypothesize that during the 150 °C dip coating process, a partial pyrolysis takes place leading to a transformation of the diethyl propyl phosphonate. Such compounds might be associated with the transformation of the aliphatic portion of the molecule detached during the dip coating, observed during the XPS analysis. If the appearance of the C=O bond induces to speculate a partial pyrolysis of the molecule during the dip coating process, during the activation step this phenomenon further proceeds, as demonstrated by the frequency shifts and by the relative intensity variation of the CH stretching modes in the range of 2800–3000 cm^{-1}.

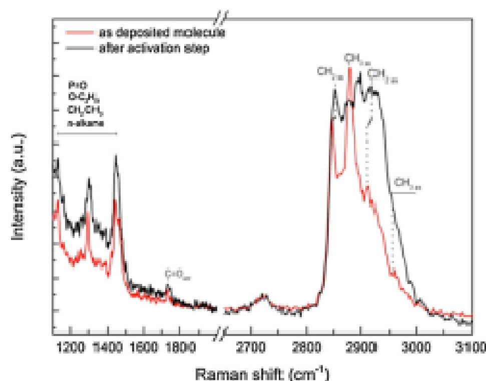

Figure 2-4 Raman spectra acquired on the as deposited sample (red line) and after the activation step in furnace at 1050 °C for 500 s in N2 (black line).

The results of the Raman analysis confirm the results obtained by XPS analysis on the fresh sample, indicating that the molecule starts to break and loss the lateral aliphatic chains during the coating process.

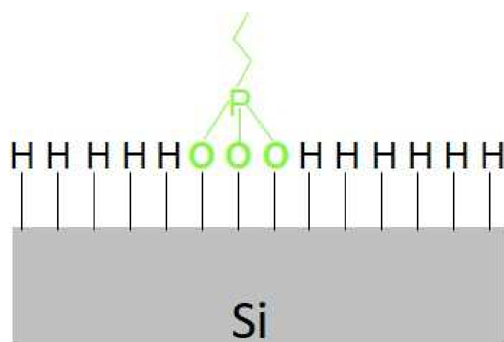

Figure 2-5 Hypothesis of a possible bond between the DPP and Silicon substrate

Figure 2-5 shows a hypothesis of the possible bond between the DPP molecule and the silicon substrate. From the results obtained by the XPS and Raman analysis and from the literature works it is possible to hypothesize that the molecule during the deposition process form a tridentate type bond with the substrate. In particular the dopant atom is bonded to the substrate via oxygen following simultaneous rupture of the C-O-P and the P = O bonds.

2.2 Role of the surface treatments

In the previous section it was found that during the deposition process for MD there is the formation of both the monolayer chemically bonded to the substrate and of the multilayers physically linked to it. In order to obtain more control on the MD process, it is important to limit the formation of the layers physically bonded to the substrate or removing them subsequently. For this reason, a series of experiments have been conducted in these two directions to remove or restrict the formation of the physi-sorbed layers.

In the literature, a study on TBAG and the possibility of removing the fused adsorbents by THF was performed with the focus of identifying multilayer vs. monolayer films [41] In MD process cleaning was applied for the first time in a work of 2011[18] in which authors removed the physi-sorbed material by rinsing the sample in ethanol, acetone, and MilliQ water and then ultrasonicated it for 15 min in acetone. In this work, no experimental evidence about the role of the cleaning on MD are present. For this reason, different cleanings were performed on the samples to fine-tune an effective removal method. Preliminary tests of cleaning in mesitylene, with increasing times from 2 minutes to 8 minutes and in water for 8 minutes were carried out. Then the samples were annealed at 1050°C for 500s and characterized by SRP to obtain an electrical measurement that can

be correlated to an indirect indication about the removal physisorbed materials. In Figure 2-6 the dose value of the samples rinsed in water and mesitylene has been plotted.

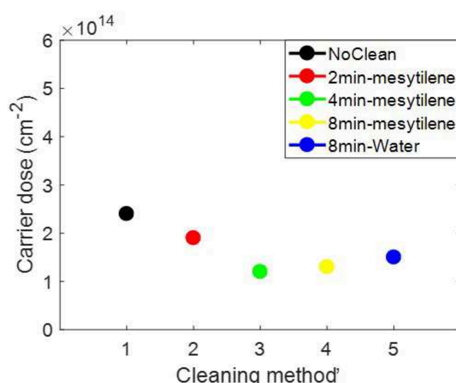

Figure 2-6 Dose obtained from SRP profiles after annealing of standard samples (no clean) and cleaned in mesitylene or water at various times.

The samples after the cleaning processes were observed with an optical microscope in order to detect the possible presence of macroaggregates (images not shown). Samples cleaned with mesitylene showed the presence of aggregates on the surface, probably due to the presence of contaminants in the solvent itself. Samples cleaned with water did not show the presence of this aggregates and for this reason it was chosen as one of the cleaning methods preferring it to the one in mesitylene. In addition to this, another method chosen was that already present in the literature and used in the MD and it consists in rinsing the sample in

ethanol, acetone, and MilliQ water and then ultrasonicated it for 15 min in acetone. Finally, the last method presents in literature where the sonication cleaning was substituted with magnetic stirring. So the samples for found a better method to remove the physi-sorbed layers were prepared in the following way: No cleaning (A), cleaning in ethanol, acetone, MilliQ water and then sonicated in acetone for 15 min (B) , cleaning in water through magnetic stirrer (C) and cleaning in acetone, isopropanol, water and 15 min in acetone under magnetic stirrer (D). After the cleaning the samples, also in this case, were annealed at 1050°C for 500s and characterized by SRP. In Figure 2-7 it is possible to note how the most effective removal method of the layers not chemically bonded to the substrate is the D case that undergone the samples to magnetic stirring.

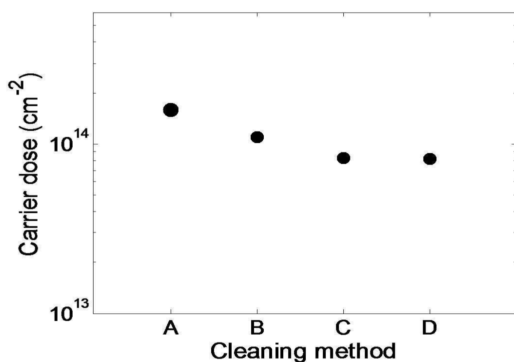

Figure 2-7 shows the plot of dose values, calculated from SRP profiles, of the various samples: no cleaning (A), cleaning in ethanol, acetone and water and sonicated in acetone (B),

cleaning with water using magnetic stirrer (C) and cleaning in acetone, isopropanol and water and then in acetone under magnetic stirrer (D).

Once the most effective removal method was found, this was chosen as a removal method for the morphological characterization of the samples. A second step was to analyze the morphological characteristic of the cleaned samples and compared it with the no cleaned samples. For this reason, the “as deposited" samples, after the cleaning cycle, was immediately characterized by morphological point of view through AFM to have an indication about the removal of the non-chemically bonded layers. In Figure 2-8 AFM microscopes are shown. The RMS was calculated for both samples to have an index of the roughness of the surface before and after the removal treatment. In Figure 2-8 a) the RMS value was of 0.740 nm while for the samples in Figure 2-8 b) the value was 0.374 nm. The RMS value in the case of the cleaned sample is considerably lower (about half), suggesting an effective removal of the physi-sorbed layers.

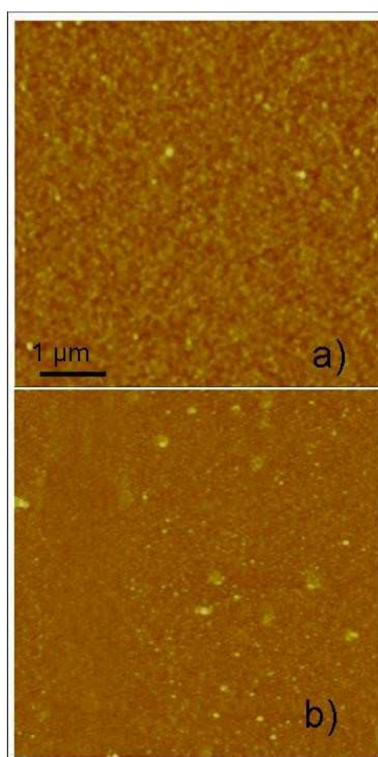

Figure 2-8 AFM micrograph of the samples no clean (a) and cleaned with acetone, isopropanol, water and acetone under magnetic stirrer (b)

The no-cleaned sample shows a total coverage of the substrate but there is the appearance of aggregates of the order of a few hundred nm. The presence of these aggregate could be caused by an increase of dopant concentration during the coating process due to the different boiling temperature between solvent and DPP. Indeed, the boiling temperature of mesitylene is about 160 °C while that of the DPP is about 280 °C. This could lead to formation of dopant aggregates on the surface during the process.

2.3 Role of the dilution of the precursor solution

In order to investigate the presence of the aggregates described in the previous paragragh a further approach consisted to decrease the concentration of DPP in mesitylene at 20,10 and 5% respectively. In this case, a systematic study was performed both morphologically and electrically at various concentrations.

The AFM images are shown in Figure 2-9 and it is seen that the surface roughness increases from the sample to 5% to 20% respectively. Specifically, the 5% sample has a Root Mean Square (RMS) of 0.250 nm. This value doubled in the case of the 10% sample (RMS 0.500 nm). Also in this sample, it is possible to note the presence of "voids" during the formation of the monolayer. The RMS value in the "voids" is different from the silicon value (0.130 nm) but very like the measured value for the sample at 5% (0.230 nm) indicating the presence of a layer already formed and that of a second layer in formation. In this case the vertical distance of the second layer was measured and the results show how the distance between the two layers is about 1 nm. In the third case, RMS was 0.740 nm. In this case there are no terraces indicating a total coverage of the substrate but there is the appearance of circular shaped aggregates the order of the hundred nm. Results from AFM images show a strong evidence about the role that DPP concentration plays in monolayer formation.

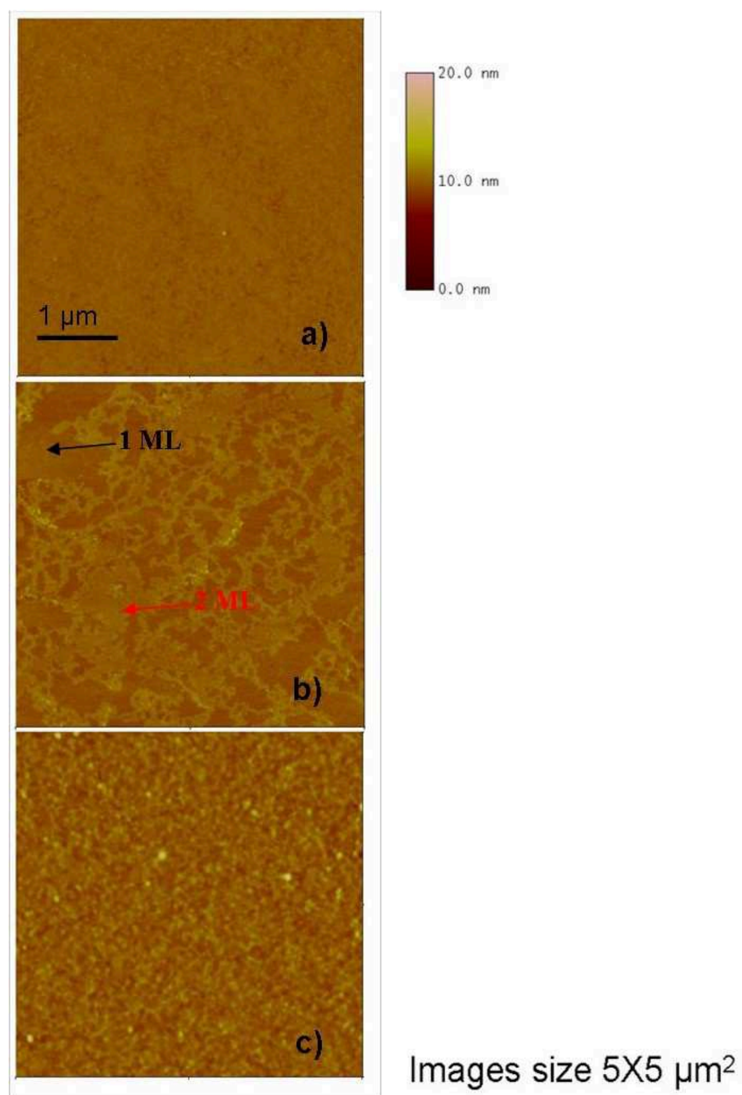

Figure 2-9 AFM microscopies carried out on samples, varying the concentration of the DPP a) 5%, b) 10% and c) 20%

Successively a set of samples processed in the same manner was characterized by SRP in order to understand the possible differences in terms of dose between the samples. Figure 2-10

shows how the dose values, calculated from the SRP profiles, are similar in the range of 5 % and 20 %, while the value of the samples at 10 % is higher. Probably because of the formation of 2nd layer that was found in AFM images. In this case the lack of formation of macromolecular aggregates allows better adhesion of the molecule to the substrate and consequently to a higher dose.

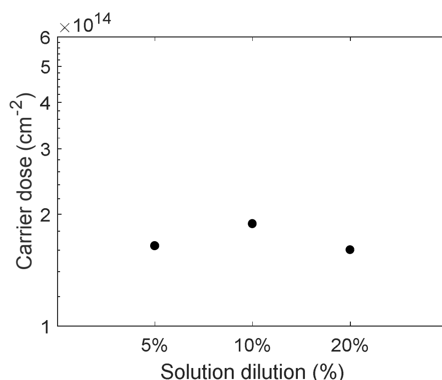

Figure 2-10 Carrier Dose value obtained by SRP profiles of the samples at various diluition of DPP

Finally, to study the removal of the physically bonded layers to vary the concentration of the molecular precursor, 2 sets of samples were prepared. The first set was prepared as deposited, cleaned with acetone, alcohol and water and then again in acetone using a magnetic stirrer and then morphologically analyzed using AFM. The second set of samples, equal to the one being analyzed AFM, was annealed after the cleaning process to get feedback from the electrical point of view. Figure 2-11 show the AFM

micrograph obtained for the cleaned samples at 5% (a), 10% (b) and 20% (c) dilution of DPP in mesitylene solution.

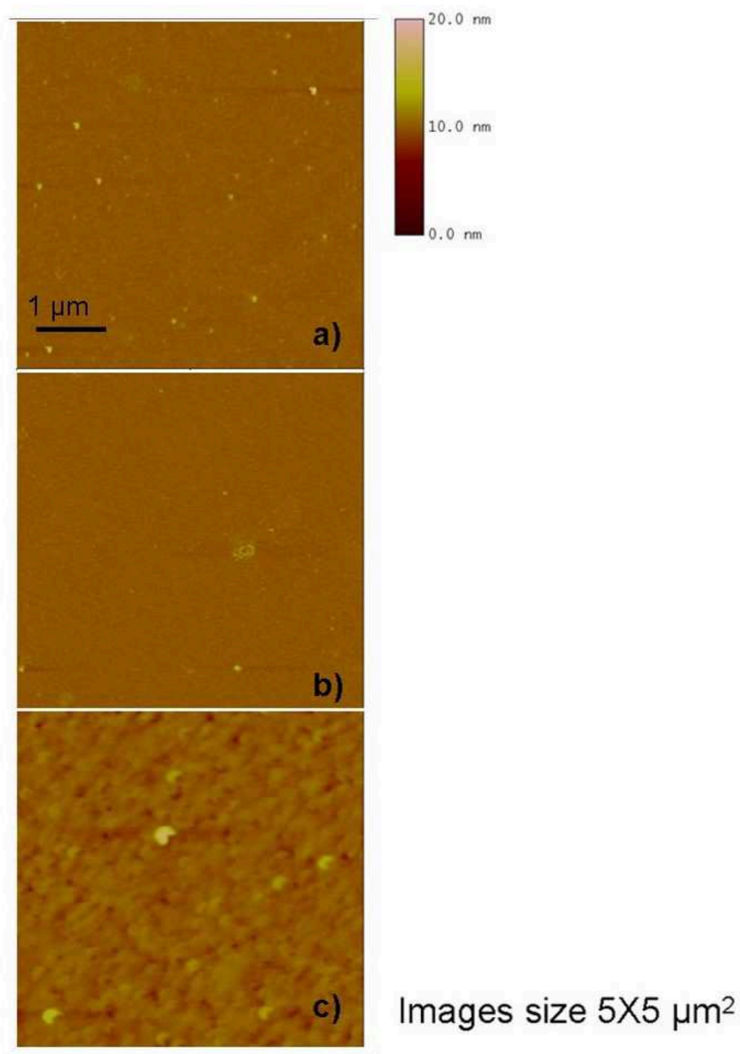

Figure 2-11 AFM microscopies carried out on "cleaned" samples, varying the concentration of the DPP a) 5%, b) 10% and c) 20%

In the first case of the sample after treatment the RMS has the same value as that of the 5% untreated sample (0.250 nm). In the second case, it becomes apparent that cleaning is effective in removing the layers physically bonded, there are no terraces indicating a total coverage of the substrate and the RMS value is equal to 5% (0.250 nm). Finally, in the third case the RMS has a value of 0.374 nm which is about half compared to that of the untreated samples. Results from AFM images strongly suggest the role that the concentration of DPP plays in the formation of the monolayer and that the subsequent dip coating treatment removes the physically attached layers. Then the second set of samples was prepared as the previous case but was annealed a 1050°C for 500 s to obtain an indirect indication about the removal of physi-sorbed layers.

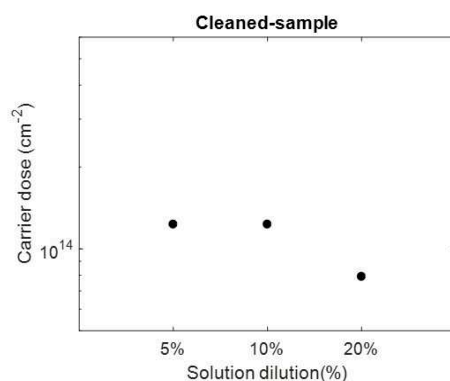

Figure 2-12 Carrier dose obtained by SRP profiles of the samples at various dilution of DPP and cleaned with acetone, alcohol and water and then again in acetone using a magnetic stirrer

Figure 2-12 show the carrier dose of the annealed samples after the MD and cleaning. In this case the value of samples at 5% and 10% was comparable and this trend confirmed the result obtained by the AFM micrograph and both cases showed a higher value than the sample at 20. This trend is due to the contribution of 2 phenomena: the first is the formation of macromolecules during the deposition phase which does not allow the best adhesion of the molecules and the second is the subsequent evaporation of the molecules itself during the annealing process.

3 Role of the deposition parameters

This chapter discusses about the role of the main deposition parameters in MD technique. The ability to modulate the main parameters corresponds to have a control over the MD deposition technique and then to have an ability to design and to prepare a sample with the desired characteristics.

In the first part of this chapter the role of coating time and sampling time will be reported. In the second part, the role of the solvent and the molecular precursor will be discussed.

3.1 Role of the coating time and sampling time

The literature on the MD doping technique shows that it is possible to modify and control the doping profile by changing the molecule design. Specifically, the molecular footprint of the precursor directly governs the surface concentration of the dopants with larger molecules resulting in a lower dose [1,34]. Starting from the results obtained in the previous chapter, where the samples show the presence of multilayers physiosorbed on the surface, a further approach was to change the immersion time of the samples in the precursor solution. For this reason, the samples were dipped first in a HF solution to remove the native oxide layer and then in a 20% v/v of DPP in mesitylene solution from 5 to 150 min. In Figure 3-1 a, the results of the SRP profiles are reported as carrier concentration versus depth for the several

coating times, all activated at 1050 °C for 500 s. As it is possible to see the profiles show a continuous increment in the junction depth until a saturation is obtained for the 100–150 min coating time. Figure 3-1 b and c show, respectively, the carrier dose and the junction depth calculated from the SRP profiles, as a function of the coating time. The trend of the charge carrier concentration and of the junction depth, as a function of dip-coating time, is monotonous. From the obtained data, it can be stated that the concentration of charge carriers and the junction depth can be precisely controlled by varying the time of coating. The results discussed above led to ask how thermal activation time affects the carrier concentration and the junction depth.

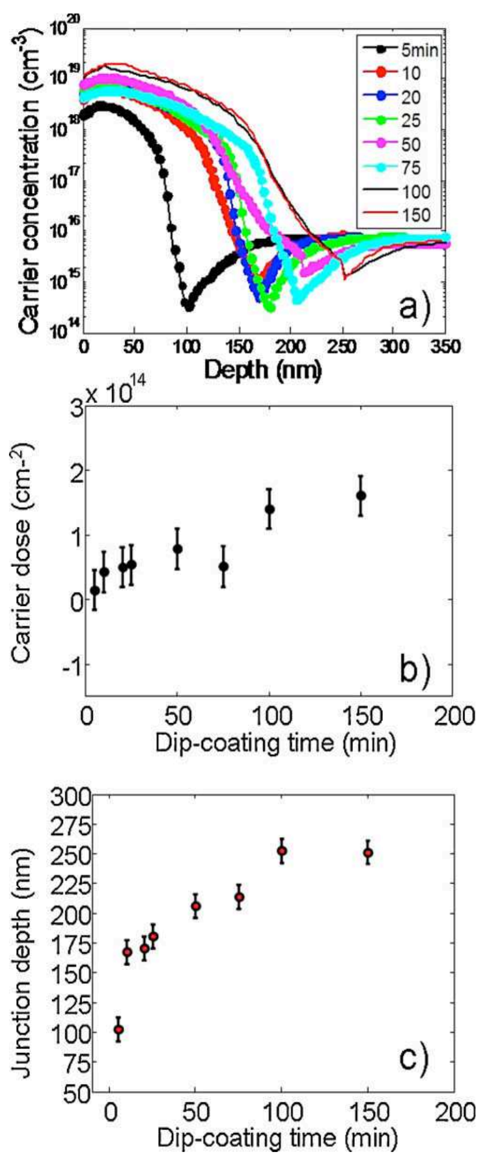

Figure 3-1 (a) Carrier concentration profiles as a function of the depth for several dip-coating times, carrier dose (b) and junction depth (c) as a function of dip-coating time.

Then the variation of DPP concentration during the process and if this variation can be responsible for the formation of the agglomerates described in the previous chapter (see Figure 2-11) is investigated. In this case the dilution is not changed by purpose but is modified during the process due to the evaporation of the solvent. For this reason, an experimental set up was carried out by processing 3 different types of samples. The samples were divided in two group for AFM and SRP characterization. All the samples were immersed in HF for the removal of native oxide and then were inserted for 25 min each, two samples were inserted at time = 0 min until time = 25 min, other two samples from time 50 min to time 75 min and finally the third group of samples was inserted at 125 min up to 150 min. One sample of each group was analyzed morphologically via AFM. (Figure 3-2) and the other one was annealed at 1050°c for 500s and then characterized by SRP. By comparing the three images (Figure 3-2 a, b and c), the formation of aggregates becomes a evident phenomenon only in the latter. This trend is even more clear by comparing the RMS numeric values: in case a) the value is 0.25 nm, in case b) it has a value of 0.550 nm while in the last case (c) the value is 0.970 nm. This phenomenon may be due to an increase in the concentration of DPP in the solution due to solvent evaporation at increasing dip coating time and consequently to its aggregation in macro-micelles depositing on the substrate.

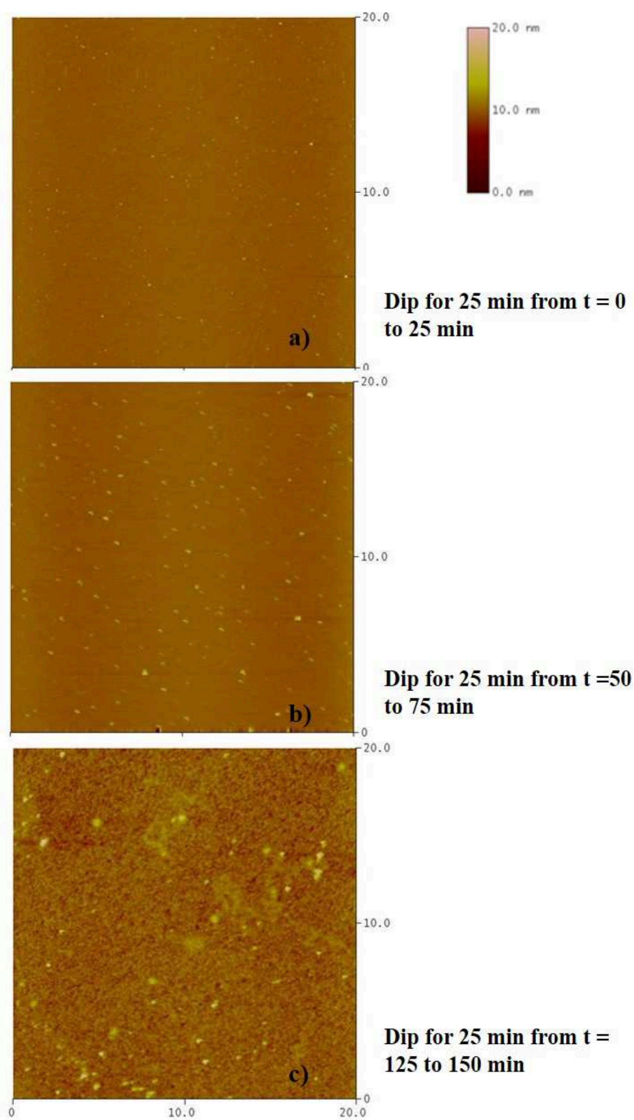

Figure 3-2 AFM micrograph performed on samples processed for the same duration of 25 min but inserted at later times in the solution.

Figure 3-3 shows the carrier dose obtained by SRP characterization of the sample immersed at different time. As can be seen, the carrier dose changes in the 3 samples. This indicates that the concentration of solution changes during the process. In particular, the trend is decreasing and this indicates a decreased ability of the molecules to adhere to the substrate surface. This result fits with those obtained through morphological analysis where we saw the appearance of macro aggregates in the sample immersed for last. These macroaggregates seem to be formed by dopant precursors, which due to micellar assembly, fail to form chemical bonds with the surface and bind to this through weak physical bonds.

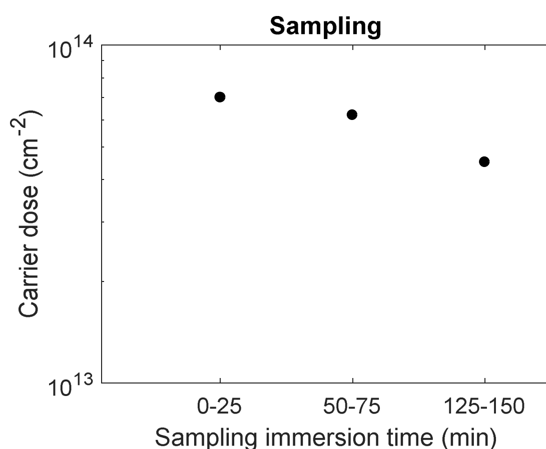

Figure 3-3 Carrier Dose from the SRP characterization of the sample after different immersion times

3.2 Role of the solvent and the molecular precursor

Another aspect investigated in this thesis was the role of the solvent and the molecular precursor at the MD. In the literature, an aspect not yet investigated concerns the variation of solvent in this type of processes. For this reason, a first aspect investigated was to replace the common solvent used in MD, mesitylene, which is an organic solvent, potentially toxic for fish and polluting for marine environments. The solvent selected to replace mesitylene should have the following characteristics: non-toxic, non-polluting, easily available, cheap, carbon-free: For this reason, we explored water as a solvent for the DPP.

Samples of Si p type with <111> crystallographic orientation was processed by MD after a brief dipping in a 16% HF solution for 60 second to remove the native oxide. After the samples were immersed in a 20% solution of DPP in water at its boiling temperature, about 120 °C for 2.5h. Then one sample before the activation thermal step was cleaned in acetone isopropanol and water and then in acetone under magnetic stirrer and finally all the samples were annealed at 1050°C for 500s. After the activation process the samples were characterized by SRP in order to obtain information about the electrical properties. Figure 3-4 shows the Carrier dose of the samples at different dilution in mesitylene (described below) cleaned or not cleaned and compared with the

samples processed using water as a solvent and also in this case undergone or not at the cleaning process.

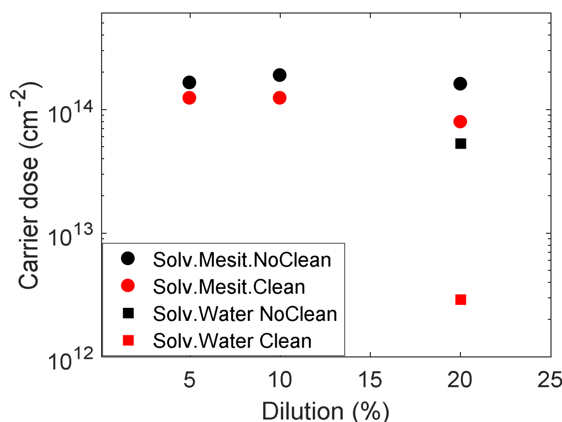

Figure 3-4 Carrier dose of the samples at different dilution in mesitylene: no cleaned (black dot), cleaned(red dot), and in water: no cleaned (black square) and cleaned (red square)

In the case of no cleaned sample the dose value is 5.3×10^{13} while in the case of the cleaned sample is 2.9×10^{12}. The value of the sample no cleaned compared to the conventional MD is about half while it is about 2 orders of inferior magnitude in the case of the cleaned sample. The cause can be attributed to the formation of a layer of oxide at the interface between the solution and the substrate before the molecule binds to this. This oxide layer limits the diffusion of molecules due to the different diffusion coefficient.

A second aspect was related to the necessity to not introduce unwanted contaminants inside the substrate during the annealing

process. In literature, any works are focused on the use of further molecular precursor but in all cases, the molecular precursors used were complex molecules in which the ratio of carbon/dopant atoms was higher than in DPP precursor[20,46]. For this reason, an innovative molecular precursor was choice to reduce the carbon atoms constituting the molecular precursor to zero. Phosphoric acid (PA) was chosen because his molecular structure is composed only of oxygen, hydrogen and phosphorus, no carbon atom is present. Also in this case, like the DPP, the phosphorus is bonded to an oxygen atom through a double bond. It is known in microelectronics because it is used in the removal of silicon nitride but which has not been, until now, as a dopant. In this case, the samples were cleaned in the following manner. Firstly, were sonicated for 5 minutes in acetone, then for 5 min in alcohol and finally for 5 min in water to remove the physical contaminants. Successively were dipped in HF solution, and then immersed in a 20% solution of Phosphoric Acid in water at 120°C for 2.5 h. Then the samples were annealed at 1050°C for 500s and then characterized by SRP. Figure 3-5 show the SRP profiles of the samples doped by Phosphoric Acid.

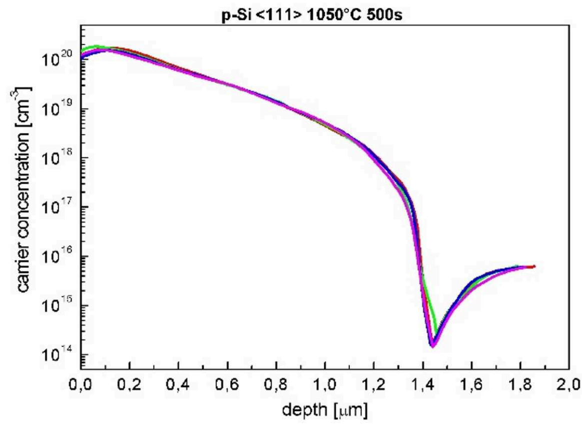

Figure 3-5 SRP profiles of samples doped by Phosphoric Acid

In this case the dose is about 6.5×10^{15} at/cm^2 and the junction depth reaches more than 1.4 microns. The differences are remarkable by comparing these samples with those doped with DPP in mesitylene (Figure 3-6).

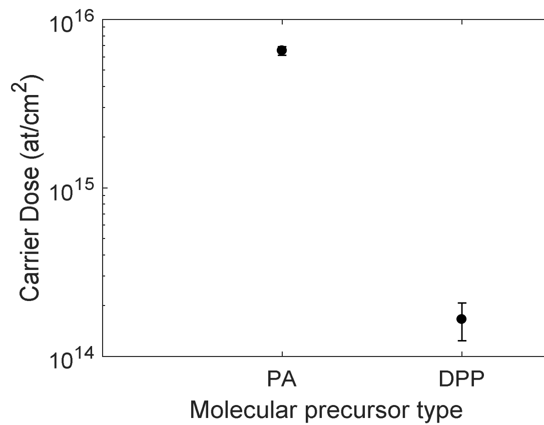

Figure 3-6 Carrier dose calculated of the samples doped by PA and DPP

Indeed, in this case the dose values are more than one order of magnitude greater, the junction depth values are about 5-6 times larger and the Rs is less than one order of magnitude. Moreover, as can be seen in the Figure 3-6, the samples doped with phosphoric acid have a lower error bar than DPP-doped samples. In order to investigate whether the spreading length of charge carriers observed in doped samples with PA can be modulated through the annealing time, a second process was performed by changing the annealing time from 500 s to 20 s. Also in this case the samples were characterized by SRP and the profiles were reported in Figure 3-7.

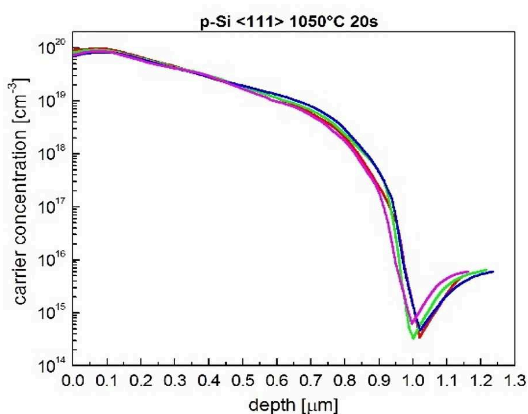

Figure 3-7 SRP profile of the samples doped by Phosphoric Acid and annealed at 1050°C for 20s.

In this case, the profiles obtained are slightly different from those scored for 500s. In fact, the dose is about half that obtained in the previous case (3×10^{15}), as well as the Rs (about 20 ohm / sq) and also the junction depth value is less (about 1 micron). Despite the

same processing conditions (temperature, time and ambient), different dose, sheet resistance and diffusion lengths have been observed compared the samples doped by PA and the samples doped by DPP. These differences could be ascribed both to the change of the molecular precursor, anomalous diffusion effects and/or to the nonlinear diffusivity at high concentrations. In order to get a qualitatively frame of the data the ideal theoretical diffusion length was evaluated (Figure 3-8 red line and dots) using the following equation:

$$L=\sqrt{2D_x t} \qquad (Eq.1)$$

using the extrinsic non-linear diffusion coefficient of P in Si:

$$D_x = D_0 + D^{--}(n/n_i)^2 \qquad (Eq.\ 2)$$

where $D_0 = 3.85\ e^{-3.66/kT}$, $D^{--} = 44.2\ e^{-4.37/kT}$, where n is approximately evaluated as the maximum carrier concentration peak in the SRP profiles and n_i is the carrier concentration of intrinsic substrate at 1050 °C[10].

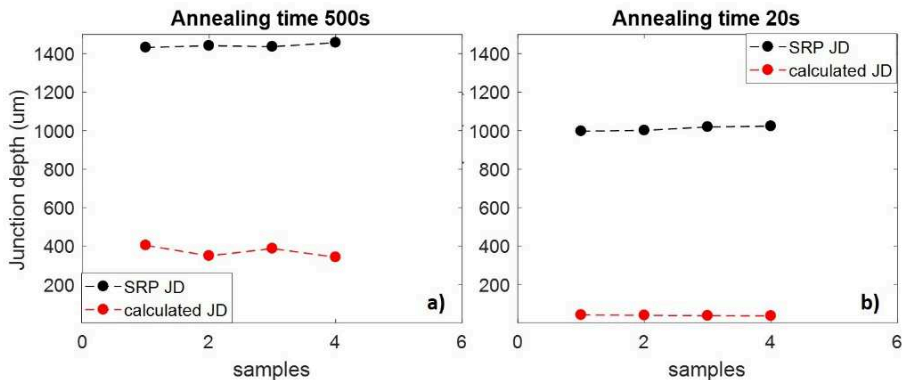

Figure 3-8 Sheet resistance results obtained by the SRP profiles as a function of the sample annealed both at 1050°C for a) 500s and b) 20s, in red the calculated diffusion length

The comparison in Figure 3-8 demonstrates that the qualitative trend of the junction depths for the different cases is remarkable. The causes could be due to several factors: first, the different dimensions of the phosphoric acid molecule compared to the DPP, second point is correlated to the concentration of molecular precursor in solution, indeed the solution was prepared using the same volume percentage of the DPP case, but in this case the number of molecules present in the solution is about 3 times greater. Finally, a further contribution probably due to the Si surface oxidation during the MD deposition and also during the annealing process, in spite to the nominally inert annealing conditions. The oxidation in fact produces a super-saturation of interstitial defects within the substrate that is responsible for a greater diffusion length [11-12].

4 Effects of the post-deposition treatments

This chapter shows the effects of the post deposition thermal process in MD.

In particular the chapter is divided in 3 parts: in the first one the role of the annealing parameters with particular attention on temperature and time was performed, in a second part an investigation about the chemical-physical properties on the surface of silicon samples after doping through molecular doping (MD) method and successive annealing is carried out. Furthermore, a study about the atomic structure of the first layers of silicon after the doping procedure in order to evaluate the possible intermixing between the carbon atoms constituting the precursor molecule and the Si atoms of the substrate is performed. Moreover, the role of this intermixed layer on the electrical characteristics of the semiconductor is also studied.

In the third part of the chapter the role on the cap layer on the MD process is discussed.

4.1 Role of the annealing parameters: Temperature and time

A route to change the doping profile characteristics is based on the modification of the thermal budget used for the dopant diffusion and activation, such as the results shown in Figure 4-1. In this figure, it reports the results of the SRP analysis performed on the Si samples after the doping procedure by using the phosphorus (Figure 4-1 a) and the boron precursor (Figure 4-1b), after the RTA diffusion step at 950 °C (red line) and 1000 °C (blue line), both for 500 s. The deposition procedure start with a brief dipping of the sample in HF, to remove the silicon native layer and then the samples were immersed in solution containing DPP or ABAPE for n or p-type doping respectively. As it is possible to see the profiles show peaks of about $1x10^{19}$ cm^{-3} of carrier concentration centered at about 10–12 nm in the first case and at 5 nm in the second case. The n+ profile depth in the P case is ≈30 and ≈80 nm after the 950 °C and 1000 °C annealing processes, respectively, while in the B case it is at ≈20 and ≈70 nm, respectively. By focusing on the boron case (Figure 4-1 b), the electrically active boron dose diffused in the bulk, as estimated by integrating the SRP profiles, is different for the two investigated cases. In the 950 °C case is found to be equal to 5×10^{12} cm^{-2}, while in the 1000 °C case is 1.5×10^{13} cm^{-2}. This difference depends on both the total dose available at the surface

in the as-prepared samples and the solid solubility of boron in silicon at that temperature, as for a standard pre-deposition process followed by a drive-in diffusion step. From the SRP measurements the sheet resistance R_s was calculated and in these cases obtained values of 3900ohm sq-1 for the sample annealed at 1000°C and 9400ohm sq-1 for the sample annealed at 950 °C. Concerning the diffusion depth, if we compare these data to the standard boron diffusion from finite sources in Si with atomically clean surfaces, i.e., without any diffusion barrier, it has been found that at such temperatures profile depths should be larger than those measured [1]. By comparing the results on the depth and on the sheet resistance to those present in the literature relative to the same chemical doping method, we find that similar values are obtained in literature for shorter annealing times than ours [1]. Many reasons have been associated with these differences: formation of a SiO_x layer before the chemical bath producing a barrier for the boron diffusion, the physico-chemical characteristics of the deposited oxide capping layer after the doping, a small penetration, up to 10 nm, of the SRP tips inside the sample that can affect the measurement, and a possible time offset due to the molecule breakage and successive boron release. These cited reasons still actually represent open issues of the molecular doping method and must be addressed by studying the chemical properties of the surface during and after the process.

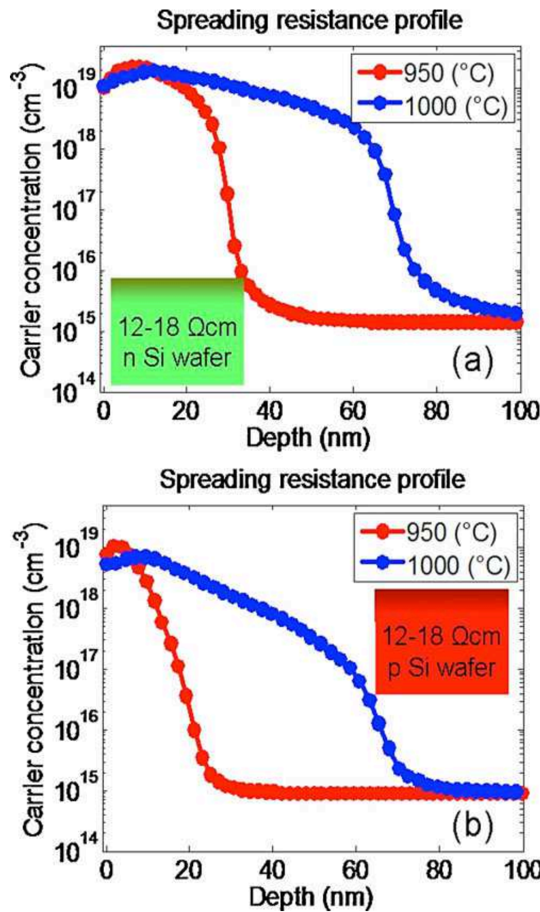

Figure 4-1 Spreading resistance profiles relative to the Si samples doped with DPP (a) and ABAPE (b) annealed at 950 °C (red) and 1000 °C (blue) for 500 s.

Finally, the contribution of the activation time on the MD was studied. In particular the activation time on samples synthesized with coating time of 150 min, was varied. The samples were subjected to a thermal activation at 1050 °C for 500 s, in a single annealing step, and 1000 s, in two steps of 500 s each, and SRP analysis were carried out. In Figure 4-2, the comparison between

the results of the two experiments are reported. The dose of the charge carriers and the junction depth, obtained by SRP profile, show that: (i) the dose of the charge carriers remains the same in both case (Φ = 1.6×10^{14} atom/ cm^3), (ii) the junction depth increases from $d_{500\ s}$ = 250 nm to d_{1000} s= 330 nm, (iii) the sheet resistance remains unchanged, R_s =300Ω/sq. The results show that after 150 min of coating time, the dose of dopant atoms diffused inside the Si substrate remains constant after increasing the diffusion time, i.e., the maximum number of P atoms has been released by the molecular layer over the Si and has diffused inside the substrate. The depth increases with time by following the diffusion process as expected.

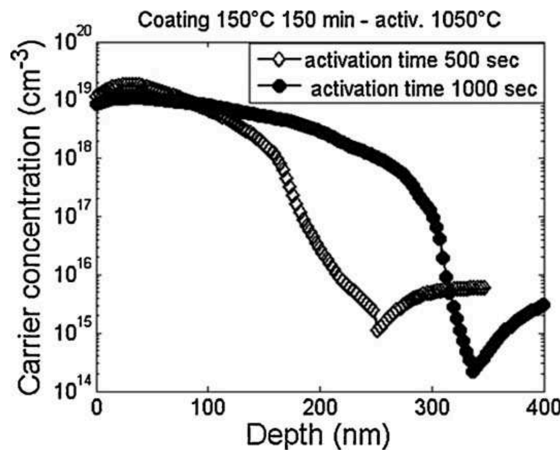

Figure 4-2 Carrier concentration profiles obtained by SRP measurements for samples coated at 150 8C for 150 min and activated at 1050 8C for 500 s (diamonds) and 1000 s (circles).

4.2 Competition between evaporation and diffusion

One very important aspect of MD is related to the role of the surface characteristics on the final electrical properties of the doped Si. It is not clear how the dose, sheet resistance and junction depth are correlated to the chemical bonds present at the surface between the Si and the atoms constituting the molecular precursor. In the literature, it was found that the atoms constituting the molecular precursor can be diffused together with the dopant atoms within the first layer of the substrate and to form a thin layer of 2-3 nm of Si-C.[47]

In this paragraph XPS has been combined with SRP analysis to understand the nature of the surface layer after the doping procedures and its role on the electrical properties. A chemical wet etch has been also performed on some samples after the doping procedure to investigate the electrical properties after the removal of a portion of surface layer [48,49]

The substrates used were p-type Si samples <111> of 1 x 1 cm^2 in size, with a R = 1-10 ohm/cm. The MD doping procedures started with a brief HF dip, immediately followed by immersion in a solution of DPP and mesitylene (20% v/v) at the solution boiling temperature, about 160 °C, for 2.5 h. This step creates a layer of phosphorus-containing molecules all over the sample surface. A

furnace annealing at 1050°C for 500sec in N_2 is then performed to diffuse and activate the dopant. In order to investigate the surface properties no cap layer has been deposited over the molecular monolayer before the annealing process. A chemical wet etch is performed to remove a portion of the surface doped layer after the diffusion step. The wet oxidation/etching process consists of 3 steps: 1) HF (16% v/v) etch is performed; 2) chemical oxidation by immersion in pure HNO_3 (63% v/v) at its boiling temperature for 10 min [48,49] 3) HF (16% v/v) dip for 120s to remove the SiO_2 layer formed during the chemical oxidation. The literature indicates that with this process the total Si etched depth corresponds to 1.6 nm. In the experiments reported in the paper, some samples have been subjected to two cycles of the oxidation/etching process to reach a nominal total etched depth of 3.2 nm.

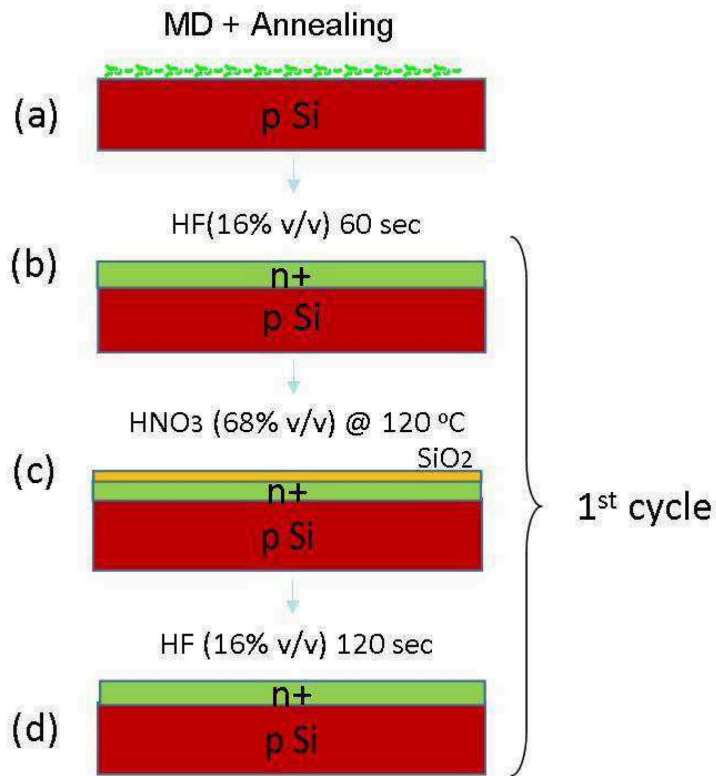

Figure 4-3 Schematic diagram of the process: a) Si p- type sample is doped by MD and annealed at 1050°C for 500 s, b) HF etching is performed for 60 sec, c) then the sample is immersed in HNO_3 at 120°C for 10 min, d) HF 16% for 60 sec.

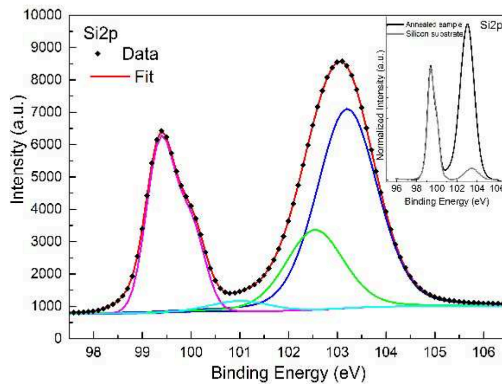

Figure 4-4: XPS spectrum relative to the signal of the Si 2p acquired on a sample after the doping and annealing process

Figure 4-4 shows the XPS spectra acquired on the sample after the MD and annealing process. The signal of the oxidized component after annealing is increased in intensity and shift to lower binding energy. The post annealing sample is also characterized by a signal at 103.5 eV due to a silicon oxide component and a multi-component band in the range of 101-104 eV that indicate the presence of different oxidation states of silicon. This behavior indicates that a silicon oxide layer is formed during the annealing process despite the process is performed in N_2 flux. By making an appropriate XPS spectrum deconvolution, it can be noted that in addition to the Si 2 p doubles (3/2 and 1/2 with values of about 0.6-0.8 FWHM eV) centered at 99.4 eV and 100 eV respectively, there is a wide band in the region of oxidized silicon species (SiO_2, SiO_x, etc.)

centered to 103.7 eV. In addition, a peak of about 100.7 eV, centered into the overlapping region, between the main peaks of silicon and oxidized species, may indicate the presence of the Si-C bond. In literature[44], the nominal position of this bond is typically between 100.6 and 101.2 eV, so this peak can be attributed to the presence of a thin layer of Si mixed with C, although it is necessary to be careful because it overlaps partially with the signal of elemental silicon at 100 eV and the energy range 101-104 eV relative to silicon oxide and substechiometric oxide species. This thin layer of Si mixed with C formed near the surface is probably due to the diffusion of the carbon atoms present in the molecular precursor during the diffusion process and in literature this literature the thickness of this layer is about 2-3 nm. This difference with the literature data is due to the processes acting on the molecular monolayer and their atomic components during the annealing process and in absence of the protective layer. In this case, they are essentially two: diffusion of the atoms constituting the precursor inside the substrate and their evaporation. In the experiments reported in the literature, the capping layer impedes the evaporation of molecular components, phosphorus, carbon and oxygen, from the surface and ensures their diffusion towards both the silicon and towards the layer of capping same. In this case, the evaporation is suppressed and the diffusion phenomenon prevails. Instead, in the reported experiments, without the protective layer, the two phenomena

become competitive. This explains the low intensity of the peak found at 100.7eV.

Figure 4-5 shows the results of SRP analysis performed after MD doping and annealing and after two cycles of oxidation/removal step. The inaccuracy of the concentration of local carrier concentration was quantified by carrying out several SRP measurements in different sample regions and a variation of about 20% was estimated. This value takes into consideration both the intrinsic value of the instrument that the irregularities of the treated sample on the surface. As can be seen, the two SRP profile show almost the same junction depth due to the limited thickness of silicon layer removed. In fact, the layer removed after the chemical processes should only be 3.2 nm thick, which is comparable to the depth of oxide removed resolution difference of the SRP analysis. The difference between the local concentration of SRP charge carriers in the two curves, in the range 0-100 nm, is at least 17%. This could be attributed to the deactivation of P induced by defective point formation during the oxidation process. Regarding the dose of charge carriers, it was calculated from the SRP profile in the pre-etch case and corresponds to a value of 1.14×0^{14} cm^{-2}, while the calculated value eliminating the first 3.2 nm of doped layer from the profile after chemical attack, corresponds to 1.09×10^{14} cm^{-2} which is 5% lower than the initial value.

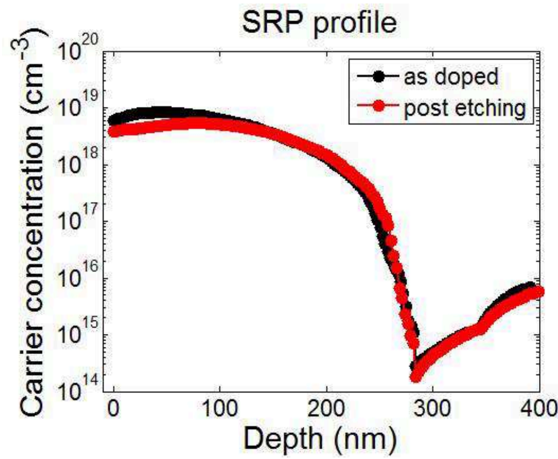

Figure 4-5 : Carrier Concentration Profiles obtained by SRP measurements on a sample after the process of doping and annealing (black curve) and on a sample after the doping process, annealing and 2 oxidation / removal cycles (red curve)

Figure 4-6 a) shows R_S values obtained by performing 4-point measurements on the sample after the doping process and after the first and second cycle of oxidation / removal process. The result indicated that after the treatments R_S increases linearly, and the variation between as doped and after the second cycle is about 7%.

Considering SRP and 4PP data, the layer removed should correspond to a few nm. In fact, as can be seen in Figure 4-6 b) TEM analysis carried out on a cross-sectional sample after the first chemical oxidation phase using HNO_3 and before removal from HF shows a thickness of oxide grown equal to 1.4-1.7 nm. This indicates that the rate of oxidation is like that expected in a

sample of pure silicon, not bound to carbon. This is in accordance with our XPS results of a low carbon content in the superficial layer. Indeed, it is known in the literature that the presence of carbon decreases the oxidation rate of Si. It should be noted that the oxidation experiment shown in Figure 4-6 b), was performed on a Si sample that was not subjected to the MD process.

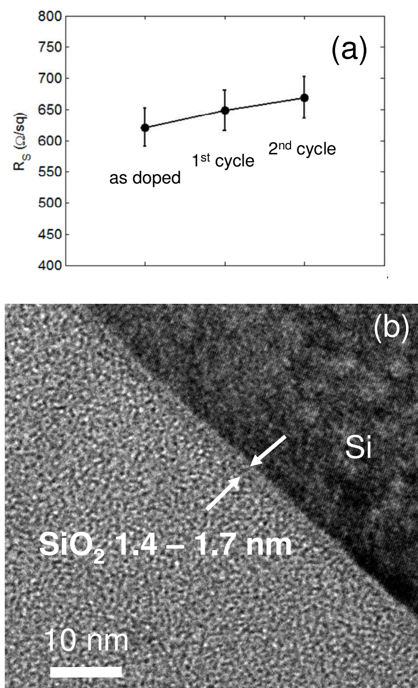

Figure 4-6 (a) Rs values obtained by 4PP measurements on samples, respectively, after the doping process and annealing (as doped), after the first cycle (1st cycle) and after the second oxidation cycle / removal (2nd cycle), (b) TEM image in cross view of the sample after the chemical oxidation process

4.3 Role of the cap layer

A further aspect investigated was the influence of cap layer on diffusion of dopant. Starting from the preliminary result obtained in the previous paragraph about the role of the cap layer. In order to thoroughly investigate which is the influence of the cap layer in MD process, a set of 4 different types of samples were prepared. The samples of Si p-type with orientation <111>, were immersed in a 16% HF solution to remove native oxide and then immersed in a 20% mesylate-based DPP solution. Then the samples were divided in 4 groups depending on the type of cap layer conditions, and named as: no cap, external cap, SOG cap and CVD cap. 'External Cap' samples correspond to samples which after the deposition of the phosphonate precursor were covered with an oxidized Si sample, placed on top of them in contact with their surface. The oxidized specimens were prepared from a Si substrate of 1cm^2 area, cleaned in acetone, alcohol, water and HF, and then thermally oxidized in a tubular furnace at 1100 °C for 46 min under 2L/min of O_2 flow. A 108 nm thick silicon oxide layer was obtained. The oxidized specimens were then placed over the MD doped layers, with the oxidized surface in contact with the precursor layer, for the annealing diffusion treatment. Regarding the 'SOG' case, after the molecular phosphonate precursor deposition, the samples have been baked at 80 °C for 60 s on a hot

plate, and then covered by SOG oxide deposited by spin coating at 3000 rpm for 20 s. A subsequent baking step at 250 °C for 60 s in air and a last annealing step in the furnace to compact the SOG layer at 425 °C for 1h under 2l/min flow of N_2 were then performed. The ‘CVD’ samples were transferred to a CVD chamber where a silicon oxide layer with a thickness of about 500 nm was deposited at using the following parameters 500W, 70°C, 10mT and 10/100sccm of a SiH_4/N_2O gas mixture. A Sentech SE 500 Ellipsometer equipped with a helium neon laser was used to measure the thickness of the several oxide layers grown or deposited on test samples. Figure 4-7 reports a schematic diagram summarizing the main processing steps for the cap layers formation after the phosphonate precursor deposition, as detailed above: Figure 4-7 a) reports the procedure for the samples annealed without cap layer; Figure 4-7 b) illustrates the steps for the ‘external cap’ samples, covered by an oxidized Si specimen obtained by thermal oxidation; in Figure 4-7 c) it is shown the procedure for the ‘SOG samples’ coated with a layer of spin on glass oxide deposited by spin coating and annealed; Figure 4-7d) details the steps for the ‘CVD’ case: the samples were coated with a 500 nm thick film of SiO_2 obtained in a plasma CVD chamber at room temperature.

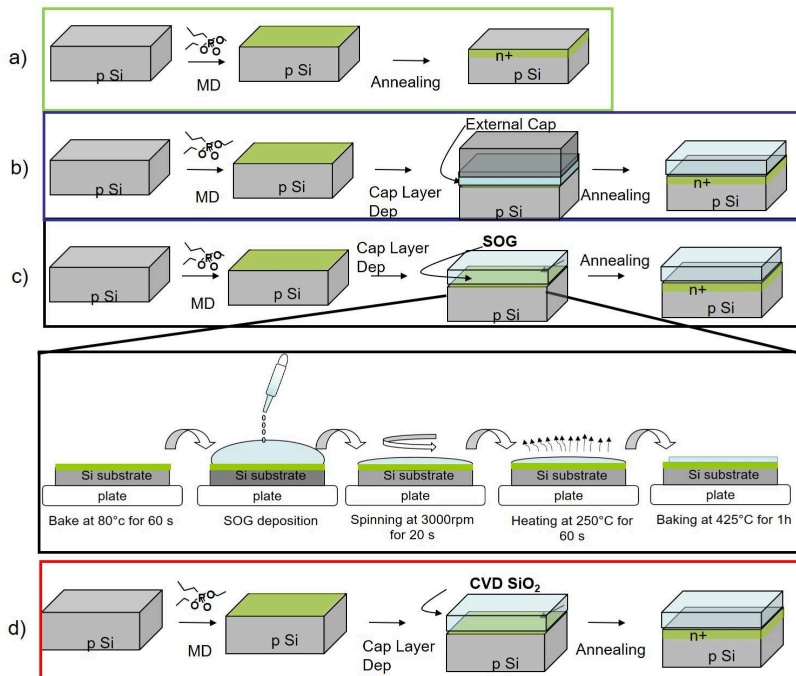

Figure 4-7 Schematic diagram of the process in which the samples after the MD deposition are covered by cap layers before the diffusion annealing: a) No Cap, b) External Cap, c) SOG Cap and d) CVD Cap

Finally, all the samples, were annealed in a furnace at 1050 °C for 500 s in N_2 flux (2 l/min) to decompose the precursor and diffuse and activate the dopant. Since the Si substrate was p-type, the diffusion process created a n+/p junction in the final samples. Spreading resistance measurements have been performed on a SSM150 tool to analyse the carrier concentration profiles in the doped samples and after the chemical processes. Depth

information is obtained by stepping down the probes along a bevelled surface of the sample. The analyses have been conducted in the high-resolution configuration, to guarantee the best accuracy for the extraction of the electrically active dopant profiles from the acquired raw data. The samples have been prepared with very small bevel angles and depth resolutions of about 3 nm have been achieved. Figure 4-8 illustrates the typical SRP profiles obtained from the samples after the diffusion step. The samples without cap layer (green curve, “No Cap”) show a peak value of the electrically active dopant concentration of ~ 1.29×10^{19} at/cm^3, in those capped by External cap the maximum concentration is ~ 1.05×10^{19} at/cm^3 (magenta curve), those coated by SOG caps show a concentration peak of ~1.49×10^{19} at/cm^3 (black curve) and finally those coated by SiO_2 obtained in CVD chamber shows a maximum concentration of ~ 2.62×10^{19} at/cm^3 (red profile). The last value is higher compared to the others.

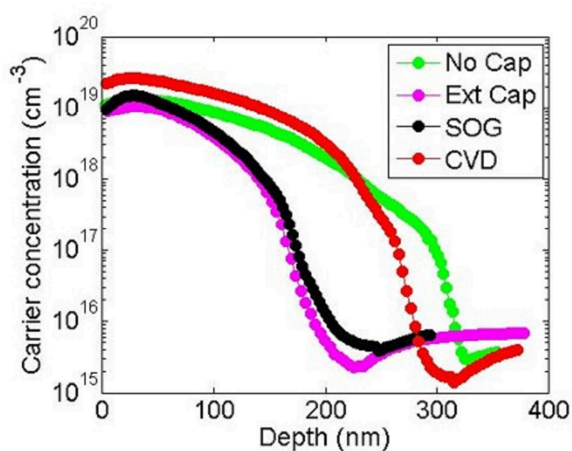

Figure 4-8 SRP profiles of samples annealed at 1050 °C for 500 s: No Cap (green curve), External Cap (magenta curve), SOG Cap (black curve) and CVD Cap (red curve)

From these profiles, we calculated the carrier dose, sheet resistance and junction depth and they are reported in fig. 3 and 4. As shown in fig 3a), the samples without cap layer show a value of carrier dose of 1.8×10^{14} at/cm^2, in the External cap samples this value is 1.1×10^{14}, in the SOG samples is 1.2×10^{14} at/cm^2, and finally the value of the CVD samples is 5.1×10^{14} at/cm^2. The reported error bars represent the standard deviation calculated on several samples treated in the same conditions. The CVD dose value is about three times larger compared to that obtained in the samples without cap layer and about five times higher than those of External cap and SOG. In Figure 4-9 b) we show the comparison among the sheet resistance average values of the four cases, calculated from the SRP dose data.

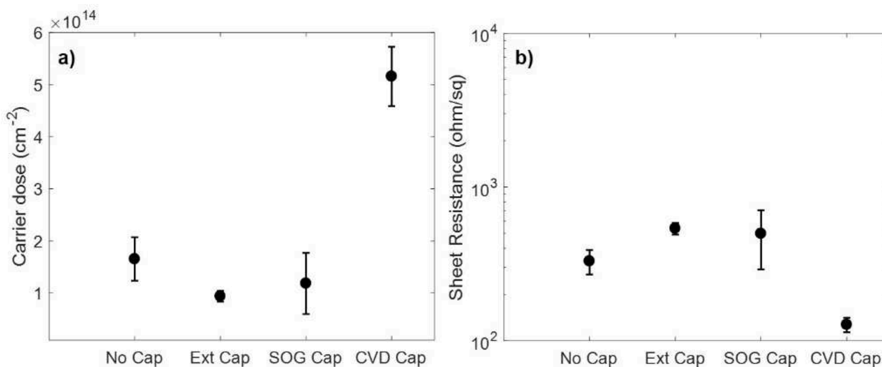

Figure 4-9 Carrier Dose (a) and Sheet Resistance (b) results obtained by the SRP profiles for the several capping conditions

The No Cap samples present a value of sheet resistance of about 3.3×10^2 ohm /sq, the External Cap samples show 5.4×10^2 ohm/sq, the value for the sample covered with SOG caps is 5.0×10^2 ohm/sq and finally for the CVD cap case is 1.3×10^2 ohm/sq. It should be noted that the sheet resistance in the samples coated by SOG oxide exhibits a larger error bar with respect to the other cases.

Also in these cases, despite the same processing conditions, different dose, sheet resistance and diffusion lengths have been observed (see Figure 4-9). These differences could be ascribed to both anomalous diffusion effects and/or to the non-linear diffusivity at high concentrations. In order to get a qualitatively frame of the data we have evaluated the ideal theoretical diffusion length (Figure 4-10 red line and dots)

$$L = \sqrt{2 D_x t} \qquad (Eq.1)$$

using the extrinsic non-linear diffusion coefficient of P in Si:

$$D_x = D_0 + D^{--}(n/n_i)^2 \qquad (Eq.\ 2)$$

where $D_0 = 3.85\ e^{-3.66/kT}$, $D^{--} = 44.2\ e^{-4.37/kT}$, where n is approximately evaluated as the maximum carrier concentration peak in the SRP profiles and n_i is the carrier concentration of intrinsic substrate at 1050 °C[50].

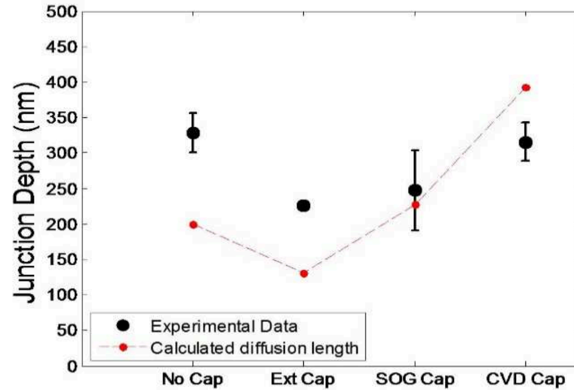

Figure 4-10 Sheet resistance results obtained by the SRP profiles as a function of the several capping conditions and calculated diffusion length

The comparison in Figure 4-10 demonstrates that the calculated qualitative trend of the junction depths for the different cases follow the trend of experimental data. The larger discrepancies are observed for the "No Cap" and "Ext Cap" cases in which show deeper diffuse profiles. In particular, the "Ext Cap" has a significantly larger diffusion than the CVD, which, in turn, shows 4 times larger active dose. This is probably due some limited Si surface oxidation during the annealing process, in spite to the nominally inert annealing conditions. The oxidation in fact produces a super-saturation of interstitial defects within the substrate that is responsible for a greater diffusion length [51,52]. For the sample covered with an outer cap layer, the non-perfect adhesion of the oxidized substrate and doped sample could make the reactivity of the Si surface more similar the no cap case.

To understand all the above results, the competition between the diffusion of the dopant towards the Si substrate and other possible loss processes which can incur during the annealing step should be considered. In the case without cap, the dopant atoms can diffuse towards the Si or evaporate in the annealing environment. The presence of the cap layer in the SOG and CVD cases makes the diffusion, both towards the substrate or the cap layer, the only possible phenomenon. The P diffusion coefficient into thermal SiO_2 is about 3 orders of magnitude less than the P diffusion coefficient in Si[13], so the P migration process towards the Si substrate is more efficient. From this, one would expect to find better electrical results in the SOG samples with respect to the 'no cap' case, which is not the experimentally observed, because depending on the density of the cap layer this process might be more efficient than the evaporation. In addition, in the case of SOG samples the molecule migration, not yet chemically bonded to the Si substrate, towards the SOG oxide precursor, still in the liquid phase before the baking steps, can be even more favoured. The large error bar exhibited in these SOG covered samples can be correlated to the non-uniform capture mechanism of the phosphonate molecules inside the liquid SOG oxide. In the case of the External cap samples evidently the non-perfect physical contact between the oxidized cap and the phosphonate covered Si samples makes loss processes active. Finally, for the CVD samples, the dopant diffusion towards the Si substrate is the

preferential process and the dopant loss processes are limited by the density of the oxide cap. This behaviour is probably due to the perfect adhesion of the cap layer on the samples that strongly restricts the out diffusion of the precursor during the annealing process.

5 Example of application to Si nanowires

Silicon nanowires (Si-NWs) have been largely recognized as promising alternative to the standard planar configuration in photodiodes, like solar cells, because they can be exploited as novel architectures to build radial junctions or as light-trapping layer for the fabrication of efficient devices [42–47]. In this case the control of the doping protocols is the difficult challenge because the common doping method need more steps to ensure conformal doping. For this reason, MD has been successfully applied to SiNWs[1,23,26]. In this section, an innovative study about the bond between the molecular precursor, DPP and the SiNWs is carried out.

SiNWs array was grown on a six inches silicon wafer, with crystallographic orientation <100>, p type 1-5 ohm cm, etched with HF solution at 16% for 60 s. After this step the wafer was introduced into sputter coater to deposit a gold catalyst by using 15 mA for 20s, at a working pressure of 5×10^{-3} mbar. A layer of 1.1×10^{16} at/cm^2 of gold was deposited in these conditions, with an equivalent layer thickness of 1.9 nm, a surface coverage of about 20% and a Au dot density in the order of 10^{11} cm^2. The wafer was then etched again by HF solution at 3% for 60 s and immediately loaded into an Inductively Coupled Plasma Chemical Vapor

Deposition (ICPCVD). The wafer holder temperature was raised up to 395°C and hold for 1h. The deposition was performed at 20W, with a chamber pressure of 20 mTorr, by using SiH_4 as Si precursor gas, with a flux of 30 sccm, and Argon as transport gas with a flux of 1sccm. The deposition time was 30 min. The wafer was then taken out of the CVD chamber and immediately subjected to a gold etch process and blow dry. After the SiNWs growth, the Si wafer was cut into pieces of 1×1 cm^2 in size and the samples were firstly morphological analyzed by scanning electron microscopy (SEM). Figure 5-1 show a SEM micrograph of the SiNWs, in planar (a) and in cross view (b). It is possible to notice that the SiNWs array show a cone shape probably due to the modification of the CVD chamber in order to obtained a better performance in terms of density of SiNWs, further investigations are needed to understand the reason and the mechanisms involved in the growth of SiNWs with this shape.

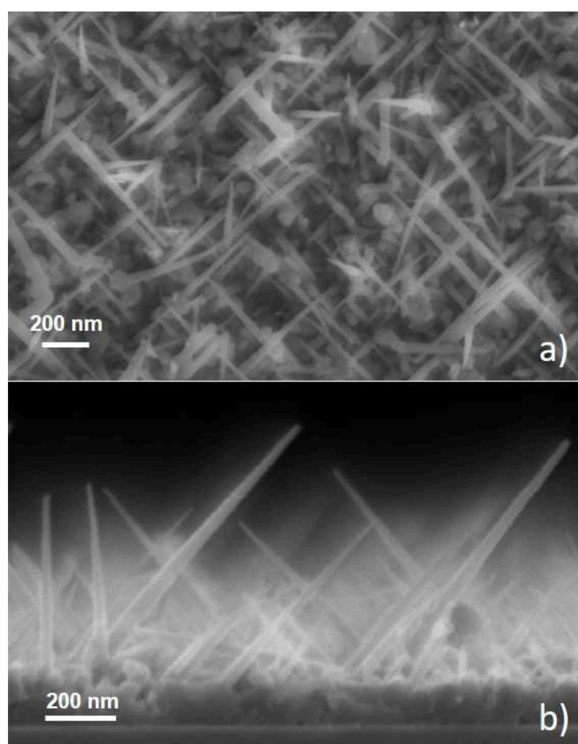

Figure 5-1 SEM micrograph of the SiNWs array a) in planar view and b) in cross view

After the morphological characterization of the SiNWs array, monolayer was created on SINWs by MD method, starting with a brief dip of the samples in a HF 16% for 60 second to remove native silicon oxide, followed by immersion in a solution of DPP and mesitylene (20% v/v) at the solution boiling temperature, about 160 °C, for 2.5 h. This step created a uniform layer of molecular precursor all over the sample surface. After the layer deposition on SiNWs array, the sample was scraped on a TEM grid and observed for morphological analysis (Figure 5-2).

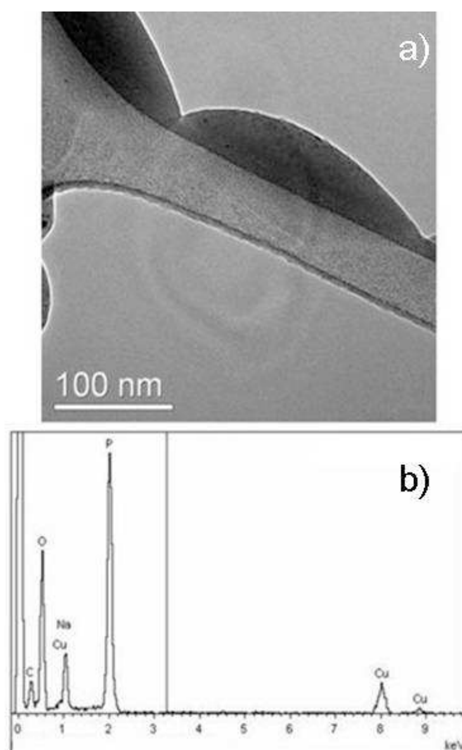

Figure 5-2 a)TEM image of DPP drpg on TEM grid and b) EDX spectrum of liquid molecule deposited on TEM grid

Figure 5-2 a) show a TEM image of a drop of a DPP deposited on TEM grid, in Figure 5-2 b) was shown the relative spectrum EDX. From the EDX spectra it is possible to note that the drop is composed mainly of phosphorus and oxygen and in this case the ratio it is not the same of the molecular precursor. The copper residues are due to the TEM grid itself. At this stage of preliminary study, a second stage of sample preparation was performed (the scheme always involves the dipping of samples in

HF to remove native oxide and subsequent immersion of the samples in the DPP solution at 20% in mesitylene for 150 minutes).

Morphological characterization and 2-dimensional chemical mapping were performed by using Transmission Electron Microscopy (TEM) in standard and scanning modes.

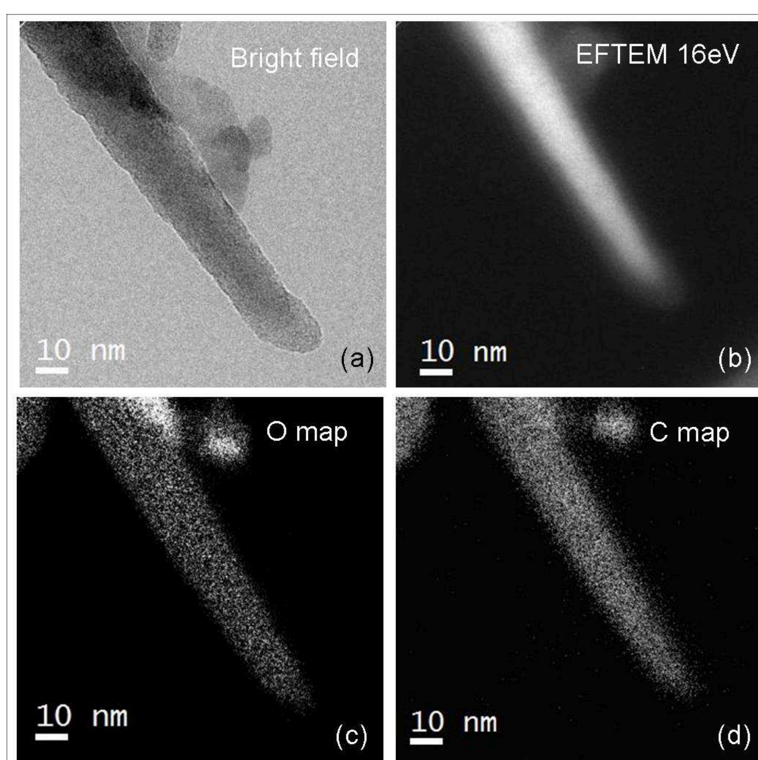

Figure 5-3 (a) Bright field TEM micrograph of a NW after the molecules deposition; (b) EFTEM image taken at 16 eV; (c) and (d) O and C maps acquired on the same region.

Figure 5-3 a) reports the low magnification bright field TEM of a NW after the molecules deposition. The EFTEM image taken at

16 eV, reported in Figure 5-3 b), indicates the Si phase inside the nanostructure. In this micrograph, the NW appears thinner than in the corresponding bright field image. Figure 5-3 c) and (d) shows the O and C maps acquired on the same region. It is evident, from the filtered images, that the C and O signals are broader than the Si one, thus suggesting the presence of layers surrounding the SiNW. EFTEM images at 16 eV were acquired by selecting in the electron energy loss spectrum (EELS) the energy window characteristic of bulk Si plasmon loss. Chemical maps for Si, C and O elements were acquired at 100, 285 and 535 eV respectively.

This type of analysis provides a low signal-to-noise ratio, not sufficient to distinguish with sub-nm accuracy the position of the different species, neither the presence of single molecules over the NW surface.

For this reason, a spectrum imaging in the scanning mode (STEM) was taken simultaneously with EELS and EDX spectra, all collected in a single multi-dimensional data matrix. The RGB image consists in the superposition of 3 chemical maps of Si, O and C, obtained from the same EELS spectrum image data-cube. This methodology allowed to extract also the low intensity EDX phosphorous signal.

Figure 5-4 a), show the results of this investigation in the region of a NW close to its tip. Due to the 3-dimensional geometry of the

analyzed nanostructure, the signal increases in correspondence of the lateral curvature, for the integration effect. The resulting image clearly evidences the separation between the two layers of O and C, red and green respectively in the image, revealing that they form two different shells. The oxygen layer is placed between Si and C and appears continuous with a thickness of about 1.2 nm. Its presence may be attributed to a native oxide regrowth after the air exposure and to a contribution from the molecular oxygen atoms. On the contrary the C signal is not continuous thus demonstrating the presence of C agglomerates of nm size (white arrows in the figure). This result is more evident in **Figure 5-4** b) showing the C map of the same NW. These agglomerates (green circles in the figure) are dimensionally compatible to the size of the single molecules.

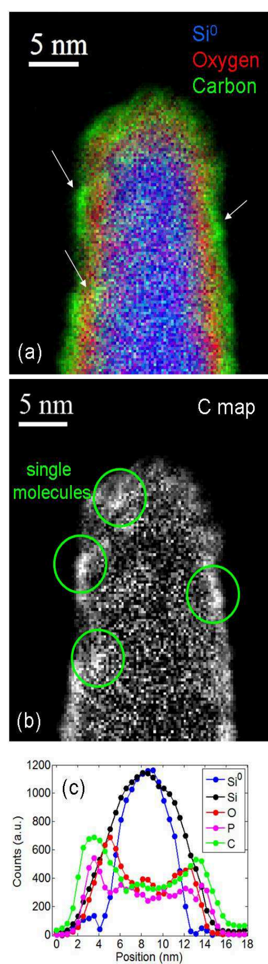

Figure 5-4 (a) RGB image extracted from the EELS spectrum image data-cube. (b) C map where the presence of the single molecule on the NW is empathized, (c) Elemental profiles extracted by the RGB spectra

6 Conclusions and future perspectives

The research activity subject of this PhD thesis has been focused on the study of innovative techniques for conformal doping of semiconductors for applications in micro- and nano-electronics.

The first part of this work was focused on the study of the interaction between the dopant molecules and Si in the solution-based MD approach because is the crucial point to be studied to deeply understand the mechanisms associated with the MD process. In the first part, an experimental investigation of MD by focusing on the chemical surface properties and on the coating process conditions was presented. The morphological and chemical characteristics of the as-deposited molecule and its interactions with the substrate are obtained by performing AFM, XPS and Raman spectroscopy with the goal to demonstrate the presence of the self-assembled monolayers and the molecule modification after the dip coating deposition and after the activation annealing. From the AFM XPS and Raman analysis it was observed that after the coating process there are both chemically bonded monolayers and non-chemically bonded multilayers. It was found that the dopant molecules are linked to the substrate with the phosphorus via an oxygen atom, probably via a tridentate-type bond. The analyses also indicated that the

molecule starts to break and loss the lateral aliphatic chains during the coating process.

Successively a series of experiments was focused on two directions: remove or restrict the formation of the physi-sorbed layers. In particular a preliminary work on different cleanings were performed on the samples to fine-tune an effective removal method and comparing two different solvents. After the deposition step, the samples processed without cleaning were directly annealed at 1050°C for 500s while the cleaned samples were cleaned before the annealing in a tubular furnace at 1050°C for 500s. Also in this case, SRP measurements were performed on all the samples and from the SRP result it is possible to note how the most effective removal method of the layers not chemically bonded to the substrate is the D case. Once the most effective removal method was found, this was chosen as a removal method for the morphological characterization of the samples. A second step was to analyze the samples after the MD coating without and with cleaning process and then were immediately characterized by AFM to have an indication about the removal of the non-chemically bonded layers. From the AFM results, RMS value was calculated in both cases. In the case of the cleaned sample is considerably lower (approximately half of the value) than the no cleaned samples, suggesting an effective removal of the physi-sorbed layers. The no cleaned samples show the presence of

aggregates of about 100 nm. To investigate this presence a further approach consisted to decrease the concentration of DPP in mesitylene at 20,10 and 5% respectively.

In this case, a systematic study was performed both morphologically and electrically at various concentrations and without or with the cleaning step. Results from AFM images strongly suggest the role that the concentration of DPP plays in the formation of the mono and multilayer and that the multilayer can be removed by the subsequent dip coating treatments. Electrical measurements indicate that the multi-layer plays an important role on the dose value. Indeed, the dose values, calculated from the SRP profiles in no cleaning samples, are similar in the range of 5 % and 20 %, while the value of the samples at 10 % is higher. Probably because of the formation of 2nd layer that was found in AFM images. The dose values in the cleaned sample are lower than the no cleaning samples and in this case the value of samples at 5% and 10% was comparable and this trend confirmed the result obtained by the AFM micrograph and both cases showed a higher value than the sample at 20. This trend is due to the contribution of 2 phenomena: the first is the formation of macromolecules during the deposition phase which does not allow the best adhesion of the molecules and the second is the subsequent evaporation of the molecules itself during the annealing process.

The second part of this work discusses about the role of the main deposition parameters in MD technique. The ability to modulate the main parameters corresponds to have a control over the MD deposition technique and then to have an ability to design and to prepare a sample with the desired characteristics.

In particular, the immersion time of the samples in the precursor solution was changed from 5 to 150 min. Then the samples were covered by SOG, annealed at 1050°C for 500s and analyzed by SRP. The trend of the charge carrier concentration and of the junction depth, as a function of dip-coating time, is monotonous. From the obtained data, it can be stated that the concentration of charge carriers and the junction depth can be precisely controlled by varying the time of coating. A second aspect about the variation of DPP concentration during the process and if this variation can be responsible for the formation of the agglomerates was investigated. In this case the dilution is not changed by purpose but is modified during the process due to the evaporation of the solvent. For this reason, an experimental set up was carried out by processing 3 different types of samples. All the samples were immersed in HF for the removal of native oxide and then were inserted for 25 min each, two samples were inserted at time = 0 min until time = 25 min, other two samples from time 50 min to time 75 min and finally the third group of samples was inserted at 125 min up to 150 min. Finally the samples were characterized

by AFM and SRP. From the AFM images on the as deposited samples the formation of aggregates becomes a evident phenomenon only in the last samples. This phenomenon may be due to an increase in the concentration of DPP in the solution due to solvent evaporation at increasing dip coating time and consequently to its aggregation in macro-micelles depositing on the substrate. The SRP trend of annealed samples is decreasing from the first to the last immersion and this indicates a decreased ability of the molecules to adhere to the substrate surface. This result fits with those obtained through morphological analysis where we saw the appearance of macro aggregates in the sample immersed for last. These macroaggregates seem to be formed by dopant precursors, which due to micellar assembly, fail to form chemical bonds with the surface and bind to this through weak physical bonds.

Another aspect investigated in this thesis was the role of the solvent and the molecular precursor at the MD. In the literature, an aspect not yet investigated concerns the variation of solvent in this type of processes. For this reason, a first aspect investigated was to replace the common solvent used in MD, mesitylene, which is an organic solvent, potentially toxic for fish and polluting for marine environments. The solvent selected to replace mesitylene should have the following characteristics: non-toxic, non-polluting, easily available, cheap, carbon-free: For this

reason, we explored water as a solvent for the DPP. In particular the samples were processed in a 20% solution of DPP in water at its boiling temperature, about 120 °C for 2.5h. Then one sample before the activation thermal step was cleaned and finally all the samples were annealed at 1050°C for 500s. After the activation process the samples were characterized by SRP. The SRP results show that the value of the sample no cleaned compared to the conventional MD is about half while it is about 2 orders of magnitude lower in the case of the cleaned sample. The cause can be attributed to the formation of a layer of oxide at the interface between the solution and the substrate before the molecules are bonded to this. This oxide layer limits the diffusion of molecules due to the different diffusion coefficient.

A second aspect was related to the necessity to not introduce unwanted contaminants inside the substrate during the annealing process. For this reason, an innovative molecular precursor was chosen to reduce the carbon atoms constituting the molecular precursor to zero. PA was chosen because his molecular structure is composed only of oxygen, hydrogen and phosphorus, no carbon atom is present. Despite the same processing conditions (temperature, time and ambient), different dose, sheet resistance and diffusion lengths have been observed compared the samples doped by PA and the samples doped by DPP. The causes could be due to several factors: first, the different dimensions of the

phosphoric acid molecule compared to the DPP, second point is correlated to the concentration of molecular precursor in solution, indeed the solution was prepared using the same volume percentage of the DPP case, but in this case the number of molecules present in the solution is about 3 times greater. Finally, a further contribution probably due to the Si surface oxidation during the MD deposition and also during the annealing process, in spite to the nominally inert annealing conditions. The oxidation in fact produces a super-saturation of interstitial defects within the substrate that is responsible for a greater diffusion length.

These are preliminary studies and will definitely require further studies to be able to control this very interesting process.

The third part of experimental results shows the effects of the post deposition thermal process in MD.

In particular the chapter is divided in 3 parts: in the first one the role of the annealing parameters with particular attention on temperature and time was performed. Si samples after the doping procedure by using the phosphorus or the boron precursor were annealed in RTA 950 °C and 1000 °C both for 500 s. The samples were analyzed by SRP and show that the n+ profile depth in the P case is ≈30 and ≈80 nm after the 950 °C and 1000 °C annealing processes, respectively, while in the B case it is at ≈20 and ≈70 nm, respectively. By focusing on the boron case if we compare the Rs data (3900 ohm/sq for the sample annealed at 1000°C and

9400 ohm/sq at 950 °C) to the standard boron diffusion from finite sources in Si with atomically clean surfaces, it has been found that at such temperatures profile depths should be larger than those measured. Many reasons have been associated with these differences: formation of a SiO_x layer before the chemical bath producing a barrier for the boron diffusion, the physico-chemical characteristics of the deposited oxide capping layer after the doping, a small penetration, up to 10 nm, of the SRP tips inside the sample that can affect the measurement, and a possible time offset due to the molecule breakage and successive boron release.

In a second part a study about the atomic structure of the first layers of silicon after the doping procedure was investigated in order to evaluate the possible intermixing between the carbon atoms constituting the precursor molecule and the Si atoms of the substrate.

In this case XPS has been combined with SRP analysis to understand the nature of the surface layer after the doping procedures and its role on the electrical properties. A chemical wet etch has been also performed on some samples after the doping procedure to investigate the electrical properties after the removal of a portion of surface layer. The result indicated that the presence of unwanted carbon contaminants is lower than in literature data due the absence of cap layer, after the

oxidation/etching treatments R_S increases linearly, and the variation between as doped and after the second cycle is about 7%.

In the third part a further aspect investigated was the influence of cap layer on diffusion of dopant. The samples were divided in 4 groups depending on the type of cap layer conditions, and named as: no cap, external cap, SOG cap and CVD cap. The better value in terms of carrier dose and sheet resistance was reported in the CVD sample cases. To understand all the results, the competition between the diffusion of the dopant towards the Si substrate and other possible loss processes which can incur during the annealing step should be considered. In the case without cap, the dopant atoms can diffuse towards the Si or evaporate in the annealing environment. The presence of the cap layer in the SOG and CVD cases makes the diffusion, both towards the substrate or the cap layer, the only possible phenomenon. In the case of SOG samples the molecule migration, not yet chemically bonded to the Si substrate, towards the SOG oxide precursor, still in the liquid phase before the baking steps, can be even more favoured. The large error bar exhibited in these SOG covered samples can be correlated to the non-uniform capture mechanism of the phosphonate molecules inside the liquid SOG oxide. In the case of the External cap samples evidently the non-perfect physical contact between the oxidized cap and the phosphonate covered Si

samples makes loss processes active. Finally, for the CVD samples, the dopant diffusion towards the Si substrate is the preferential process and the dopant loss processes are limited by the density of the oxide cap. This behaviour is probably due to the perfect adhesion of the cap layer on the samples that strongly restricts the out diffusion of the precursor during the annealing process.

Finally an innovative study about the bond between the molecular precursor, DPP, and the SiNWs is carried out. The SiNWs was growth by VLS method using gold as a catalyst, then the MD was performed on it and successively a morphological characterization was performed. The RGB image extracted from the EELS spectrum image clearly evidences the separation between the layers of O and C revealing that they form two different shells. The oxygen layer is placed between Si and C and appears continuous with a thickness of about 1.2 nm. Its presence may be attributed to a native oxide regrowth after the air exposure and to a contribution from the molecular oxygen atoms. On the contrary the C signal is not continuous thus demonstrating the presence of C agglomerates of nm size. These agglomerates are dimensionally compatible to the size of the single molecules.

Further investigations on SiNWs samples doped with MD after the annealing step are needed to better understand the process.

Appendix

X-Ray Photoelectron Spectroscopy: XPS

XPS is a chemical analysis technique of solid state materials: it is based on the analysis of the energy of secondary electrons emitted by a material following an excitation promoted by energy photons in the X-ray range. Technique allows to obtain information about the type, amount and state of oxidation of elements present in the first surface nanometers of a material. The photoemission can be summarized in three main phases: first, incident X-rays interact with the solid electronic shells by generating both photoelectrons emitted for either photoelectric or electrons emitted by Auger slit. Part of these electrons will be able to get out of the material and be emitted into the vacuum of the room of the apparatus, along with a harmful component, generated by anaelastic scattering processes to which the electrons have taken part in the path of exit from the material. Therefore, the main information that the technique will provide us will be the kinetic energy of electrons emitted by the material that is analyzed by an "electronic energy analyzer", in particular a semisphere concentric analyzer.

The process is described by the Einstein relation:

$h\nu = BE + KE + \phi S$

where ν is the frequency of the incident irradiation, BE the Binding Energy of the electron, with respect to the vacuum level, ϕS work function and KE the Kinetic Energy of the photoelectron.

Considering that the analyst's work function is experimentally determined through a reference sample, the only amount to be determined for each experiment is the kinetic energy of the photoelectric electron, as the energy of the incident photon is known. In fact, the instrument uses two sources for X-rays: they are the MgK_{α} emission lines (with energy equal to hν = 1253.6 eV, with a peak width of 0.70 eV) and AlK_{α} (with energy equal to hν = 1486.6 eV, With a peak width of 0.85 eV). Electrons that are analyzed have a "Binding Energy" of just a few hundred eV and therefore cannot penetrate a solid for long walks due to their energy loss, which is described by their "Inelastic mean free path". This implies that the electrons emerging from the surface of the sample will come from layers near the surface and that the detected signal will be composed mostly of surface components.

The photoelectron peaks appear to specific BE values for each element, however, it is also function of the chemical around of the atom and its oxidation state, hence, it is possible to identify also more complex chemical species.

In this thesis, the XPS analysis were obtained by a K-Alpha system from Thermo Scientific, equipped with a monochromatic Al Kα source (1486.6 eV), and operating in constant analyser

energy (CAE) mode with a pass energy of 200 and 50 eV for survey and high-resolution spectra, respectively. A spot size diameter of about 400 μm was adopted. The binding energy was calibrated by the elemental Si2p peak centered at 99.3 eV for silicon substrate. Measurements were carried out at 90° take-off angles between the sample surface and the direction of photoelectrons detected by the analyzer. Curve fitting of the core-level XPS lines was carried out using XPSpeak41 software with a Gaussian–Lorentzian product function and linear Shirley background subtraction. A Gaussian–Lorentzian mixing ratio was taken as 0.15 for all lines.

Spreading Resistance Profiling: SRP

Spreading Resistance Profiling (SRP) retains its popularity in the semiconductor industry by an inexpensive means of capturing dopant profile information. SRP is a method to measure the resistivity of semiconducting samples as a function of position. Two metal needles spaced about 50 µm apart are pressed with a force of about 100 µN (10 mg) against the surface of the semiconductor and the resistance between these two needles is measured. Spreading resistance (SR) is the resistance associated with a divergent current passing between electrodes on the surface of a semiconductor material. This quantity is determined by applying a known current between the electrodes on the surface of the sample and measuring the voltage drop between the probes.

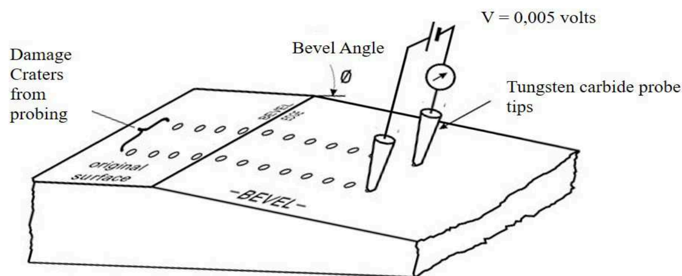

Figure 0-1 Schematic of a SRP measurements

Figure 0-1 shows a simple two-probe spreading resistance measurement system. A structure's carrier concentration profile is measured by angle lapping the sample and making a series of SRP

measurements along the bevel. Profile depth is calculated as a function of the bevel angle. Correction factors are used to convert the spreading resistance values to carrier concentration levels. The technique of using spreading resistance to measure the thickness of diffused layers and impurity profiles was originally proposed by Mazur and Dickey in 1966.

In this thesis SRP measurements have been performed by a SSM150 tool to analyse the carrier concentration profiles in the doped samples. The analyses have been conducted in the high-resolution configuration, to guarantee the best accuracy for the extraction of the electrically active dopant profiles from the acquired raw data. The samples have been prepared with very small bevel angles and depth resolutions of about 3 nm have been achieved.

Atomic Force Microscopy: AFM

AFM is a technique to obtain images and other information from a wide variety of samples, at extremely high (nanometer) resolution. AFM works by scanning a very sharp (end radius ca. 10 nm) probe along the sample surface, carefully maintaining the force between the probe and surface at a set, low level. Usually, the probe is formed by a silicon or silicon nitride cantilever with a sharp integrated tip, and the vertical bending (deflection) of the cantilever due to forces acting on the tip is detected by a laser focused on the back of the cantilever. The laser is reflected by the cantilever onto a distant photodetector. The movement of the laser spot on the photodetector gives a greatly exaggerated measurement of the movement of the probe. This set-up is known as an optical lever. The probe is moved over the sample by a scanner, typically a piezoelectric element, which can make extremely precise movements. The combination of the sharp tip, the very sensitive optical lever, and the highly precise movements by the scanner, combined with the careful control of probe-sample forces allow the extremely high resolution of AFM. The basic principle of AFM is that a probe is maintained in close contact with the sample surface by a feedback mechanism as it scans over the surface, and the movement of the probe to stay at the same probe-sample distance is taken to be the sample topography. A variety of probes have been used but the most commonly used are

microfabricated silicon (Si) or silicon nitride (Si_3N_4) cantilevers with integrated tips. Typically, probe radius varies from 5 to 20 nm. The bending of the cantilever normal to the sample surface is usually monitored by an optical lever, although other methods have been investigated. This system magnifies the normal bending of the cantilever greatly, and is sensitive to Angstrom-level movements. There are a variety of modes of scanning but in the simplest mode, the probes gently touch the sample as it moves over the surface. The movement of the probe over the surface is controlled by a scanner. This is normally made from a piezoelectric material, which can move the probe very precisely in the x, y, and z axes, although other types of actuator are also used. The signal from the photodetector passes through a feedback circuit, and into the z movement part of the scanner, in order to maintain the probe-sample distance at a set value. Because the cantilever acts as a spring, this fixed cantilever deflection means a fixed probe-sample force is maintained. The amount by which the scanner must move in the z axis to maintain the cantilever deflection is taken to be equivalent to the sample topography.

In this thesis, the AFM technique was used in order to obtain a morphological information of the samples as prepared.

Raman Spectroscopy

Raman spectroscopy is a molecular spectroscopy, which is observed as inelasticaly scattered light and enables the interrogation and identification of vibrational (phonon) states of molecules. Therefore, Raman spectroscopy provides an invaluable analytical tool for molecular finger printing and for monitoring changes in molecular bond structure, for example, state changes and stresses and strains. Raman spectroscopy has several major advantages over vibrational spectroscopy techniques, such as FT-IR and NIR. These advantages stem from the fact that the Raman effect manifests itself in the light scattered off of a sample as opposed to the light absorbed by a sample. Therefore, Raman spectroscopy is insensitive to aqueous absorption bands and requires little sample preparation. This characteristic of Raman spectroscopy enables the measurement of gases, liquids, and solids not only directly, but also through transparent containers such as plastic, glass, and quartz. Similar to FT-IR, Raman is highly selective, allowing it to detect and distinguish between molecules and chemical species that are very similar. When considering Raman scattering, the physics can be thought about in one of two ways: the classical wave interpretation or the quantum particle interpretation. In the classical wave interpretation, light is considered as electromagnetic radiation, which consists of an oscillating electric field that interacts with a molecule through its

polarizability. Polarizability is measured by the ability of an electron cloud to interact with an electric field. For example, soft molecules such as benzene have the tendency to be strong Raman scatterers, whereas harder molecules like water tend to be fairly weak Raman scatterers. When considering the quantum particle interpretation, light is considered a photon, which strikes the molecule and then inelasticaly scatters. In this interpretation, the number of scattered photons is proportional to the size of the bond. For instance, molecules with large Pi bonds such as benzene have the tendency to scatter lots of photons, while water with small single bonds is often a very weak Raman scattered.

In this thesis Raman analysis were performed by using the 514.5 nm radiation of an Ar ion laser. Scattered light has been confocally collected and analysed by a Jobin–Yvon 450mm monochromator equipped with a CCD detector cooled at 77 K.

Transmission Electron Microscopy

The transmission electron microscopy is a commonly used technique to study the structural properties of materials at atomic level resolution. A high energy beam of electrons is shone through a very thin sample, and the interactions between the electrons and the atoms can be used to observe features such as the crystal structure and features in the structure like dislocations and grain boundaries. Chemical analysis can also be performed. TEM can be used to study the growth of layers, their composition and defects in semiconductors. High resolution can be used to analyze the quality, shape, size and density of quantum wells, wires and dots. The TEM operates on the same basic principles as the light microscope but uses electrons instead of light (Figure 0-2a). Because the wavelength of electrons is much smaller than that of light, the optimal resolution attainable for TEM images is many orders of magnitude better than that from an optical microscope. Thus, TEM can reveal the finest details of internal structure - in some cases as small as individual atoms. The beam of electrons from the electron gun is focused into a small, thin, coherent beam by the use of the condenser lens. This beam is restricted by the condenser aperture, which excludes high angle electrons. The beam strikes the specimen and part of it is transmitted depending upon the thickness and electron transparency of the specimen. This transmitted portion is focused by the objective lens into an image on phosphor screen or charge

coupled device (CCD) camera. Optional objective apertures can be used to enhance the contrast by blocking out high-angle diffracted electrons. The image then passed down the column through the intermediate and projector lenses, is enlarged all the way.

The image strikes the phosphor screen and light is generated, allowing the user to see the image. The darker areas of the image represent those areas of the sample that fewer electrons are transmitted through, while

the lighter areas of the image represent those areas of the sample that more electrons were transmitted through.

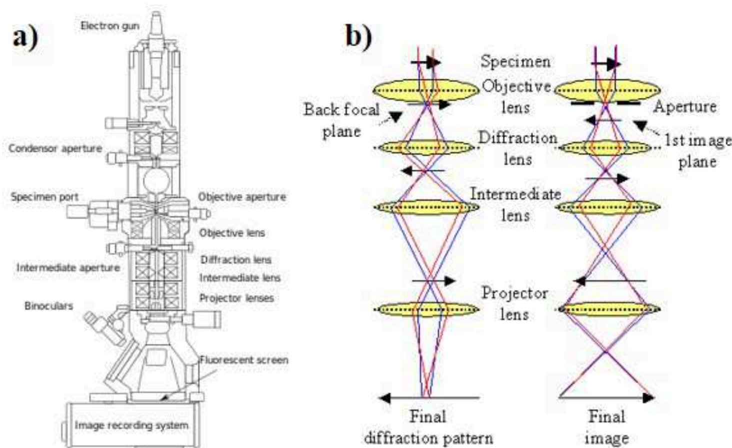

Figure 0-2 a) General layout of a TEM describing the path of electron beam in a TEM, b) a ray diagram for the diffraction mechanism in TEM.

Figure 0-2 b shows a simple sketch of the path of a beam of electrons in a TEM from just above the specimen and down the column to the phosphor screen. As the electrons pass through the sample, they are scattered by the electrostatic potential set up by the constituent elements in the specimen. After passing through the specimen they pass through the electromagnetic objective lens, which focuses all the electrons scattered from one point of the specimen into one point in the image plane. Also, shown in Figure 0-2 b is a dotted line where the electrons scattered in the same direction by the sample are collected into a single point. This is the back focal plane of the objective lens and is where the diffraction pattern is formed.

In this thesis, TEM characterization was performed by a FEG-TEM JEOL 2010F microscope and JEOL ARM 200, equipped with a cold FEG, aberration corrected condenser lens, JEOL 100 mm^2 Energy Dispersive X-ray (EDX) detector and Gatan Quantum Spectrometer. The instrument provides during a single scan a dark field image with High Angle Annular Dark Field (HAADF) detector, simultaneously with EELS and EDX spectra, all collected in a single multi-dimensional data matrix.

This technique was used to obtain morphological information on SiNWs samples after the monolayer deposition.

References

1. Ho, J. C. *et al.* Controlled nanoscale doping of semiconductors via molecular monolayers. *Nature Publishing Group* **7,** (2008).

2. Puglisi, R. A. *et al.* Molecular doping applied to Si nanowires array based solar cells. *Solar Energy Materials and Solar Cells* **132,** 118–122 (2015).

3. Sietmann, R., Mainwood, A., Newton, M. E., Stoneham, M. & Jenkins, T. A brief history of . . . semiconductors. *Physics Education* **40,** 430–439 (2005).

4. Moore, G. E. Cramming more components onto integrated circuits. *Proceedings of the IEEE* **86,** 82–85 (1998).

5. Frank, D. J. *et al.* Device scaling limits of Si MOSFETs and their application dependencies. *Proceedings of the IEEE* **89,** 259–287 (2001).

6. Gibbons, J. F. Ion implantation in semiconductors-Part II Damage production and annealing. *Proceedings of the IEEE* **60,** 1062–1095 (1972).

7. Williams, J. S. Ion implantation of semiconductors. Materials Science & Engineering, A: Structural Materials: Properties, Microstructure and Processing **A253,** 8–15 (1998).

8. Hieslmair, H., Mandrell, L., Chun, M., Latchford, I. & Adibi, B. Advantages of ion-implantation for solar cells. *Proceeding of the 25th European Photovoltaic Solar Energy Conference and Exhibition / WCPEC-5, Valencia, Spain* 1252–1256 (2010).

9. Chu, P. K., Qin, S., Chan, C., Cheung, N. W. & Larson, L. A. Plasma immersion ion implantation - A fledgling technique for semiconductor processing. *Materials Science and Engineering R: Reports* **17,** 207–280 (1996).

10. Cheung, N. W. Plasma immersion ion implantation for semiconductor processing. *Materials Chemistry and Physics* **46,** 132–139 (1996).

11. Gupta, D. Plasma immersion ion implantation (PIII) process-physics AND technology. *International Journal of Advancements in Technology* **2,** 471–490 (2011).

12. Yu, M. L., Vitkavage, D. J. & Meyerson, B. S. Doping reaction of PH3 and B2H6 with Si(100). *Journal of Applied Physics* **59,** 4032–4037 (1986).

13. Flemish, J. R. & Tressler, R. E. Phosphorus Doping of Silicon Using a Solid Planar Diffusion Source at Reduced Pressures. *J. Electrochem. Soc.* **138,** 233–238 (1991).

14. Kuisl, M. & Sasse, E. Diffusion of Phosphorus in silicon dioxide from a spin-on source. *Thin Solid Films* **65,** 373–380 (1980).

15. Polignano, M. L., Picco, P. & Cerofolini, G. F. Phosphorus silica glass as dopant source. *Journal of the Electrochemical Society* **127,** 2734–2738 (1980).

16. Cerofolini, G. F. *et al.* Phosphorus diffusion into silicon from chemically vapour-deposited phosphosilicate glass. *Thin Solid Films* **87,** 373–378 (1982).

17. Arduca, E. *et al.* Synthesis and characterization of P δ - layer in SiO 2 by monolayer doping. *Nanotechnology* **27,** 75606 (2016).

18. Voorthuijzen, W. P., Yilmaz, M. D., Naber, W. J. M., Huskens, J. & Van Der Wiel, W. G. Local doping of silicon using nanoimprint lithography and molecular monolayers. *Advanced Materials* **23,** 1346–1350 (2011).

19. Puglisi, R. A. *et al.* A comprehensive study on the physicochemical and electrical properties of Si doped with the molecular doping method. *Physica Status Solidi (A) Applications and Materials Science* **212,** (2015).

20. Alphazan, T. *et al.* Monolayer Doping of Silicon through Grafting a Tailored Molecular Phosphorus Precursor onto Oxide-

Passivated Silicon Surfaces. *Chemistry of Materials* **28,** 3634–3640 (2016).

21. O'Connell, J. *et al.* Organo-arsenic Molecular Layers on Silicon for High-Density Doping. *ACS Applied Materials and Interfaces* **7,** 15514–15521 (2015).

22. Ho, J. C. *et al.* Wafer-scale, sub-5 nm junction formation by monolayer doping and conventional spike annealing. *Nano Letters* **9,** 725–730 (2009).

23. Puglisi, R. A. Towards Ordered Silicon Nanostructures through Self-Assembling Mechanisms and Processes. *Journal of Nanomaterials* **2015,** (2015).

24. Garozzo, C. *et al.* Radial junctions formed by conformal chemical doping for innovative hole-based solar cells. *Materials Science and Engineering B: Solid-State Materials for Advanced Technology* **178,** 686–690 (2013).

25. Garozzo, C. *et al.* Nanofabrication processes for innovative nanohole-based solar cells. *Physica Status Solidi (A) Applications and Materials Science* **210,** 1564–1570 (2013).

26. Veerbeek, J. *et al.* Highly doped silicon nanowires by monolayer doping. *Nanoscale* **27,** 6781–6796 (2017).

27. Hazut, O. *et al.* Contact doping of silicon wafers and nanostructures with phosphine oxide monolayers. *ACS Nano* **6,** 10311–10318 (2012).

28. Sun, Z. *et al.* Dopant diffusion and activation in silicon nanowires fabricated by ex situ doping: A correlative study via atom-probe tomography and scanning tunneling spectroscopy. *Nano Letters* **16,** 4490–4500 (2016).

29. Neves, B. R. A., Salmon, M. E., Russell, P. E. & Troughton, E. B. Spread coating of OPA on mica: From multilayers to self-assembled monolayers. *Langmuir* **17,** 8193–8198 (2001).

30. Ekerdt, J. G., Klabunde, K. J., Shapley, J. R., White, J. M. & Yates Jr, J. T. Surface chemistry of organophosphorus compounds. *The Journal of Physical Chemistry* **92,** 6182–6188 (1988).

31. Hanson, E. L., Schwartz, J., Nickel, B., Koch, N. & Danisman, M. F. Bonding Self-Assembled, Compact Organophosphonate Monolayers to the Native Oxide Surface of Silicon. *Journal of the American Chemical Society* **125,** 16074–16080 (2003).

32. Slaoui, A. *et al.* Rapid Thermal Diffusion of Phosphorus into Silicon from Doped Oxide Films. in *22nd IEEE Photovoltaic Specialists Conference (PVSC)* 445–449 (1991). doi:10.1109/PVSC.1991.169255

33. Spampinato, V. *et al.* Functionalization of oxide surfaces by terpyridine phosphonate ligands: Surface reactions and anchoring geometry. *Langmuir* **26,** 8400–8406 (2010).

34. Ho, J. C. *et al.* Nanoscale doping of InAs via sulfur monolayers. *Applied Physics Letters* **95,** 8–11 (2009).

35. Barnett, J. *et al.* Advanced techniques for achieving ultra-shallow junctions in future CMOS devices. *IWJT-2010: Extended Abstracts - 2010 International Workshop on Junction Technology* **78741,** 132–135 (2010).

36. US20050147750A1.pdf.

37. Hoque, E. *et al.* Phosphonate self-assembled monolayers on aluminum surfaces. *Journal of Chemical Physics* **124,** (2006).

38. Hoque, E., DeRose, J. A., Bhushan, B. & Hipps, K. W. Low adhesion, non-wetting phosphonate self-assembled monolayer films formed on copper oxide surfaces. *Ultramicroscopy* **109,** 1015–1022 (2009).

39. Nie, H.-Y., Walzak, M. J. & Mcintyre, N. S. Substrate Studied by Atomic Force Microscopy. *Langmuir* **18,** 2955–2958 (2002).

40. Nie, H., Walzak, M. J. & Mcintyre, N. S. Delivering Octadecylphosphonic Acid Self-Assembled Monolayers on a Si Wafer and Other Oxide Surfaces Delivering Octadecylphosphonic

Acid Self-Assembled Monolayers on a Si Wafer and Other Oxide Surfaces. *Society* 21101–21108 (2006). doi:10.1021/jp062811g

41. Gouzman, I., Dubey, M., Carolus, M. D., Schwartz, J. & Bernasek, S. L. Monolayer vs. multilayer self-assembled alkylphosphonate films: X-ray photoelectron spectroscopy studies. *Surface Science* **600,** 773–781 (2006).

42. Branch, B. *et al.* Investigating phosphonate monolayer stability on ALD oxide surfaces. *Applied Surface Science* **288,** 98–108 (2014).

43. Yerushalmi, R., Ho, J. C., Fan, Z. & Javey, A. Phosphine oxide monolayers on SiO2 surfaces. *Angewandte Chemie - International Edition* **47,** 4440–4442 (2008).

44. Moulder, J. F., Stickle, W. F., Sobol, P. E. & Bomben, K. D. Handbook of X-ray Photoelectron Spectroscopy. *Surface And Interface Analysis* **3,** v–v (1979).

45. Fujii, M., Sugimoto, H., Hasegawa, M. & Imakita, K. Silicon nanocrystals with high boron and phosphorus concentration hydrophilic shell - Raman scattering and X-ray photoelectron spectroscopic studies. *Journal of Applied Physics* **115,** (2014).

46. Wu, H. *et al.* Controlled doping by self-assembled dendrimer-like macromolecules. *Scientific Reports* **7,** 41299 (2017).

47. Shimizu, Y. *et al.* Behavior of phosphorous and contaminants from molecular doping combined with a conventional spike annealing method. *Nanoscale* **6,** 706 (2014).

48. Kobayashi Asuha, H., Maida, O., Takahashi, M. & Iwasa, H. Nitric acid oxidation of Si to form ultrathin silicon dioxide layers with a low leakage current density. *Journal of Applied Physics* **94,** 7328 (2003).

49. Imamura, K. *et al.* Nitric acid oxidation of Si method at 120 °c: HNO3 concentration dependence. *Journal of Applied Physics* **107,** 1–6 (2010).

50. Misiakos, K. & Tsamakis, D. Accurate measurements of the silicon intrinsic carrier density from 78 to 340 K. *Journal of Applied Physics* **74,** 3293–3297 (1993).

51. Shibata, Y., Hashimoto, I. S., Taniguchi, K. & Hamaguchi, C. Oxidation Enhanced Diffusion of Phosphorus over a Wide Range of Oxidation Rates Diffusion. *J. Electrochem. Soc.* **139,** (1992).

52. Jones, S. W. Diffusion in silicon. *Journal of Applied Physics* **38,** 3475 (2000).

53. Garnett, E. & Yang, P. Light trapping in silicon nanowire solar cells. *Nano Letters* **10,** 1082–1087 (2010).

54. Garnett, E. C. & Yang, P. Silicon nanowire radial p-n junction solar cells. *Journal of the American Chemical Society* **130,** 9224–9225 (2008).

55. Tsakalakos, L. *et al.* Silicon nanowire solar cells. *Applied Physics Letters* **91,** (2007).

56. Garnett, E. & Yang, P. D. Light Trapping in Silicon Nanowire Solar Cells. *Nano Letters* **10,** 1082–1087 (2010).

57. Wang, F. *et al.* A high efficiency and cost effective Si thin film solar cell with novel periodic nanohole textured surface. in *2010 Photonics Global Conference, PGC 2010* (2010). doi:10.1109/PGC.2010.5706071

58. Moulin, E. *et al.* Thin-film silicon solar cells with integrated silver nanoparticles. *Thin Solid Films* **516,** 6813–6817 (2008).

Acknowledgements

Publications

- R. A. Puglisi, S. Caccamo, C. Bongiorno, G. Fisicaro, L. Genovese, S. Goedecker, G. Mannino, and A. La Magna, Direct observation of organic single molecules grafted to the silicon nanowire surface, To be submitted

- S. Caccamo, M. G. Grimaldi, M. Italia, A. La Magna, G. Mannino and R. A. Puglisi, Applied Physics Letters, To be submitted (APL17-AR-08300)

- R. A. Puglisi, V. Lombardo and S. Caccamo (2017), "Silicon quasi-1Dimensional nanostructures for photovoltaic applications", Review Chapter, number 7, pages 131-153, in the Book: "Nanowires – New Insights", ISBN 978-953-51-5257-6, Editor: Dr. Khan Maaz, Intech

- V. Indelicato, S. Caccamo, E. Fazio, A. La Magna and R. A. Puglisi, Activity Report 2016, Dipartimento di Scienze Matematiche ed Informatiche, Scienze Fisiche e Scienze della Terra, ISSN 2038-5889, pages 97 – 100, (2016)

- R. A. Puglisi, S. Caccamo et al. Phys. Status Solidi A 212, No. 8, 1685–1694 (2015)

- S. Caccamo, R. A. Puglisi et al. Materials Science in Semiconductor Processing (2015), Materials Science in Semiconductor Processing 42 (2016) 200–203

Conferences

-Talk Author EMRS 2017 European Material Research Society, May 22-26 2017, Strasbourg, France

- Talk Author Nanosea, 3rd to the 8th of July, *2016* Giardini Naxos, Messina, Italy

- Talk Author Materials 2016, December 12 th to 16 th, *2016* Acicastello, Catania, Italy

- Talk Author EMRS 2016 European Material Research Society, May 2- 6 2016, Lille, France

- Presenting Poster EMRS 2016 European Material Research Society,May 2- 6 2016, Lille, France

- Presenting Poster at FISMAT 2015 Italian National Conference on Condensed Matter Physics September 28 - October 2, 2015 Palermo Italy